In form for a swarm: programmable neutrophil swarming impacts infection outcome

Salik M. Borbora[1§], Ivanna Williantarra[1§], Giulia Rinaldi[1], Tuhin Samanta[2], Can Cui[1], Echo Yongqi Luo[1], Hazel A. Walker[1], Debsuvra Ghosh[2], Holly M. Craven[1,3], Auxence Desrentes[1], Nir S. Gov[1,2], Milka Sarris[1*]

Affiliations:

[1]Department of Physiology, Development and Neuroscience, University of Cambridge, Downing Site, Cambridge, CB2 3DY, UK.

[2]Department of Chemical and Biological Physics, Weizmann Institute of Science, Rehovot, Israel

[3]Roving Researcher Programme, School of Biological Sciences, University of Cambridge, United Kingdom

§ These authors contributed equally

*Correspondence to: ms543@cam.ac.uk

Abstract

Migrating cells often pattern the distribution of chemoattractants to support their accumulation in target tissues. Neutrophil swarming represents a prominent example in which cells engage in coordinated paracrine chemoattractant signalling for rapid clustering at sites of injury or infection. Whether neutrophil swarming can be regeared to influence immune outcomes is unclear. Here, we show that neutrophil swarming is subject to reprogramming after microbial experience and amenable to genetic enhancement with measurable effects on infection outcome. We demonstrate that zebrafish larvae exposed to prior microbial experience are trained to be more resistant to subsequent wound infection. Through live imaging and chemical perturbations, we show that these training effects are in part attributed to changes in neutrophil swarming and associated gene expression signatures. Among the reprogrammed genes, genetic enhancement of 5-lipoxygenase is sufficient to maximise neutrophil swarming and improve infection outcome. Finally, through mathematical modelling, we demonstrate that alterations in attractant secretion, sensitivity of bacterial detection and stop signals predict kinetics of neutrophil swarming and bacterial clearance in trained animals. Together, these data suggest new routes for reprogramming cell accumulation and positioning in tissues, via manipulating their ability to shape chemoattractant landscapes.

Introduction

Directed cell migration is essential for tissue development and surveillance. Guidance of migrating cells relies on interpretation of gradients of chemoattractants within tissues. Traditional mechanistic models portray migrating cells as receivers of information, responding to chemoattractant landscapes patterned by extrinsic tissue cells. However, several lines of evidence highlight an important role for self-organisation in the process, through cell-autonomous generation of chemical gradients by migratory cells[1–5]. For example, during development, migrating tissue collectives sculpt chemical gradients through asymmetric distribution of dedicated chemoattractant scavenging receptors[3,5]. In cancer metastasis, melanoma cells disperse via catabolism of ligand and local micro-gradient generation[6]. In chemotactic mazes, amoeboid cells detect dead ends using breakdown of chemoattractant[7]. During immune responses, leukocytes pattern autologous chemical gradients through chemoattractant scavenging or through autocrine/paracrine secretion[8–12]. Finally, modification of ligands by migrating cells can generate complex patterns such as reverse chemotaxis[13]. A fundamental question raised by these observations is whether cell guidance is autonomously programmable, in a manner sufficient to impact disease at the tissue and organism scale.

To explore this question, we focus on the prominent paradigm of neutrophil swarming, as a self-organised migration behaviour. Neutrophils are first responders to tissue injury and infection and directly fight microbes through a variety of effector mechanisms, such as phagocytosis, secretion of antimicrobial molecules, and release of neutrophil extracellular traps (NETs)[14]. Neutrophils also produce chemokines and cytokines that influence the accumulation and function of other cells and ultimately shape the course of inflammation and disease. The recruitment of neutrophils is initially prompted by primary signals produced by tissue cells afflicted by injury or infection[14]. Thereafter, neutrophils begin to secrete further chemoattractants, generating tissue-scale gradients and/or waves of chemoattractants, which amplify the range of recruitment and determine the final magnitude of the response[8–11,15–17]. The process of neutrophil swarming is highly conserved and thought to impart functional benefits in fighting infection, particularly in the face of large and focal targets, such as wound infection or fungal invasions[9,18,19]. Specifically, swarms are characterized by rapid kinetics of recruitment and dense accumulation of neutrophils[8–11,15], which in principle would support prompt containment of pathogens, physical insulation of the pathogen-afflicted area and local

concentration of antimicrobial molecules. On the other hand, neutrophil accumulation is also known to prolong pathological inflammation when not properly regulated and resolved[14,20]. Therefore, the mechanisms and rules of organisation underlying neutrophil swarm development have important functional implications in disease.

Several conserved mechanisms have been determined that drive the initiation and evolution of neutrophil swarming. This includes the key neutrophil-derived chemoattractants driving swarm development (notably, the eicosanoid leukotriene B4 (LTB4) and the chemokine Cxcl8[8,9,15,21]), signal inducers of chemoattractant secretion (such as coordinated calcium signals[9,10,22]) as well as factors that self-limit the evolution of swarms (such as receptor desensitization and reactive oxygen species[10,23,24]). Additional contributing factors have also been described, such as damage associated molecular patterns (for example ATP and fMLP[9,11]) and cellular behaviours, such as neutrophil NETosis and target cloaking by other immune cells[21,25]. Despite the overall conservation of neutrophil swarming and associated mechanisms, the dynamics of neutrophil swarm behaviours within a given experimental system show significant heterogeneity, ranging from small, short-lived clusters, to persistent and larger clusters[9,26]. Although some of this heterogeneity can be attributed to variation in the intensity and composition of tissue-derived signals[23,25], it remains unclear whether cell-intrinsic properties account for variation in neutrophil propensity to swarm and whether these are subject to re-programming.

Immune cell gene expression and function can be re-programmed in at least two ways. The first is through experience and 'training', whereby immune cells exposed to a primary insult acquire epigenetic marks that poise their gene expression profile and responsiveness to a subsequent insult[27–29]. Neutrophils have been shown to undergo such durable training after exposure to primary infection, through epigenetic re-programming in relevant long-lived progenitors[30,30–33]. Innate immune training increases resistance to infection in a variety of tumour and infection settings and involves a range of epigenome and transcriptome changes[30,31,34,35]. Whilst it is well-established that neutrophils enhance their killing capacity and associated gene signatures after immune training[30,36–38], it remains unclear to what extent their ability to swarm can also undergo re-programming under these conditions. A second route to re-programming immune function is through genetic engineering, as exemplified in tumor immunotherapies. Specifically, chimeric antigen receptors (CAR) can be engineered in immune cells to programme their ability to recognise and kill certain tumours[39]. Whilst this has been developed to the largest extent for T lymphocytes[39], new approaches for CAR therapies

are geared towards the manipulation of myeloid cells, including macrophages and neutrophils[40–43]. However, the ability to genetically reprogramme the infiltration of immune cells to target diseased tissues remains a challenging frontier. In this context, the manipulation of self-generated gradients is a relatively unexplored but interesting route of manipulation, as it offers the potential to modify the composition of inflammatory niches through the reprogramming of ligands delivered by immune cells to the site.

Here we exploit the zebrafish as a tractable model to explore the link between cell behaviours at the microscopic with disease outcome at the whole-organism scale. We developed and characterised a model of wound infection in which neutrophil swarm heterogeneities can be visualized in real time in individual animals, concomitant with monitoring of disease progression and infection outcome. We first establish factors that determine susceptibility of wound infection, notably the role of osmotic surveillance programmes in the epithelial barrier. We then show that training challenge of zebrafish with non-pathogenic microbes enhances resistance to subsequent wound infections and that, under these conditions, neutrophils exhibit enhanced swarming prowess with reduced swarm heterogeneity across individuals. We found that this correlates with upregulation of swarm-related gene expression signatures and that inhibition of swarm machinery (LTB4 biosynthesis pathway) limits the protective effects of prior microbial insult. We show that targeted genetic enhancement of swarm machinery enhances neutrophil swarming and resistance to wound infection, indicating that neutrophil swarm reprogramming is sufficient to influence infection outcome. Finally, we show that mathematical modelling predicts distinct mechanisms of swarm reprogramming and associated benefits in bacterial clearance in 5-LO engineered neutrophils versus in neutrophils from microbially trained animals.

Results

Tissue damage detection through osmotic surveillance shapes susceptibility of zebrafish larvae to pathogenic wound infections

To investigate the dynamics and functional consequences of neutrophil swarms, we employed a wound infection model. *Pseudomonas aeruginosa* is an opportunistic bacterial pathogen, present in water and soil, able to colonise wounds in multiple species. In humans, wound infections can occur through contact of injured tissue with contaminated water or surfaces[44,45]. These infections can be severe and lead to sepsis and mortality, particularly in immunocompromised individuals or in the case of large surgery-associated infections[44,45]. We previously introduced a model whereby zebrafish larvae are subjected to wounding in the presence of aqueous medium contaminated with *P. aeruginosa* PAO1 strain[9]. This experimental model is advantageous in that it recapitulates a natural route of infection, in comparison to more common microinjection routes[46], and provides a relevant setting to study the role of neutrophil swarming in defence. However, these experimental infections are inherently more variable, since heterogeneities in the injured tissue can influence the titres of microbial colonisation and the ensuing immune response.

To understand and control sources of variation in this model, we examined known aspects of the tissue response to damage. Previous studies have shown that damage detection through osmotic surveillance is important for epithelial wound closure[47], inflammatory signal production and recruitment of neutrophils[48]. In addition, these tissue damage detection pathways were shown to promote optimal defence from microbes, when the latter are microinjected into hosts[49]. We therefore aimed to establish whether wound infections are influenced by osmotic surveillance pathways, with a view to minimising variation in infection.

To test the role of osmotic surveillance, we subjected zebrafish larvae to two types of wounding, mechanical and laser wounding **(Fig. 1A, G)**, in two common zebrafish buffers E3 medium (hypotonic), Ringer medium (isotonic), as well as isotonic E3 medium (with the same sodium levels and tonicity as Ringer). The use of two wounding assays offers complementary advantages. Whilst mechanical wounding can be performed on a large scale, to screen for disease phenotypes, laser wounding permits real-time visualisation of neutrophil responses

170 immediately upon wounding[9,50]. In both types of wound assays, we found that larvae in
171 hypotonic medium were largely resistant to wound infection, whereas larvae in isotonic
172 medium (iso E3, Ringer) were susceptible **(Fig. 1E, H)**. In all media conditions, non-wounded
173 larvae were resistant to infection, confirming the wound-dependent nature of infection **(Fig.**
174 **1E, H)**. To characterise the disease progression in a more granular fashion, we created a disease
175 scoring matrix, with phenotypes ranging from alterations in swimming behaviour, to more
176 extensive morphological abnormalities **(Fig. 1B)**. Larvae infected in hypotonic media showed
177 minimal disease symptoms and bacterial burdens in comparison to larvae infected in isotonic
178 media (**Fig 1C, J)**.
179
180 Wound closure can be delayed in isotonic media due to lack of tissue damage detection by the
181 ruptured epithelium[47]. We hypothesised that this may render wounds more permissive to
182 bacterial colonisation, contributing to the increased burden of infection in these conditions
183 **(Fig. 1D, I)**. We confirmed in our experimental setting that wound closure was delayed in
184 isotonic solutions (**Fig. S1A and B**, **Movie S1**). In addition, we observed a trend for reduced
185 neutrophil recruitment in isotonic solutions, consistent with previous reports (**Fig. S1C**). To
186 test whether early wound colonisation might differ in the different media, we measured
187 bacterial burden shortly after wound infection (10 min and 30 min), at time points shorter than
188 the duplication time of *P. aeruginosa*[51]. We found that at this early stage the bacterial titres
189 were already significantly higher in isotonic conditions, suggesting either a difference in
190 bacterial colonisation or a difference in the early containment by immune cells **(Fig. 1F)**. To
191 test direct effects of the medium composition on the growth of bacteria, we examined the
192 growth of PAO1 bacteria in hypotonic E3, isotonic E3, Ringer and PBS solutions. We found
193 comparable bacterial growth after 30 min exposure in the different media, suggesting that the
194 disease phenotypes of the larvae depended on the host response (**Fig. S1D**, **Movie S1**).
195
196 Together these results indicated an important role for osmotic surveillance in wound defence
197 and allowed us to establish the optimal conditions for recapitulating wound infection and
198 associated disease in larvae.
199
200 **Training through microbial challenge alters neutrophil swarm-related gene expression**
201 **and enhances resistance to wound infections**
202

203 We thereafter used the susceptible model of wound infection (isotonic conditions for
204 infection/Ringer solution) to explore whether we can reprogramme the innate immune response
205 to infection through training. To mimic vaccination challenge, we used superficial
206 microinjection as a route. We injected non-pathogenic, CFP-expressing *Escherichia coli*
207 MG1655[52] in the otic vesicle at 2 days post-fertilisation **(Fig. 2A)**. We found this pre-challenge
208 increased the resistance to wound infection by *P. aeruginosa*, two days after the first challenge,
209 as compared with controlled PBS-pre-challenged larvae **(Fig. 2B)**. Notably, in the absence of
210 wounding, larvae were not susceptible to infection in either PBS *or E. coli*-pre-challenge,
211 confirming again the opportunistic nature of infection **(Fig. S2A)**. Varying the dose of *E. coli*
212 injection showed that a minimum dose was required to trigger protective effects **(Fig. S2B)**.
213 One way of distinguishing innate immune 'training' from immune 'priming' is by assessing
214 whether the protective effects persist after the immune response to the first challenge has passed
215 its peak or resolved. To explore the nature of the protection observed, we determined the
216 resolution kinetics of the first challenge, by measuring titres of *E. coli* and levels of
217 inflammatory cytokines **(Fig 2E)**. Both markers indicated that the response to *E. coli* had
218 largely subsided by the time the second challenge was given **(Fig 2F-J)**.
219
220 Neutrophil training is characterised by changes in transcriptomic and epigenetic signatures in
221 differentiated neutrophils and progenitors[33]. Since the training challenge led to resistance of
222 infection in a heterologous tissue site (tail versus ear), we hypothesised neutrophils from
223 hematopoietic sites might be centrally altered. To explore this, we isolated neutrophils from the
224 caudal hematopoietic tissue (CHT) **(Fig. 2K)** and found that CHT-derived neutrophils showed
225 increased expression of genes associated with inflammation and cell migration, in particular
226 *cxcl8a*, *5-lo* and cytoskeletal proteins, such as *tubg1* **(Fig 2L-R)**. This suggested that
227 neutrophils may be centrally altered by training in a manner that changes their gene expression
228 profile.
229
230 To explore epigenetic changes in genes associated to swarming, we mined published datasets
231 in models of neutrophil training by *S. flexneri,* which is phylogenetically highly related to
232 *E.coli*[53 38]. Zebrafish neutrophils undergo epigenetic reprogramming upon sub-lethal *Shigella*
233 *flexneri* infection, and this is associated with enhanced resistance to subsequent *S. flexneri*
234 infection. We explored whether swarm-associated genes undergo epigenetic modification in
235 this model and found that H3K4me3 marks were induced in *Shigella*-trained animals in gene

236 loci associated to LTB4 synthesis and production, namely *5lo/alox-5*, *lta4h* and *cyp4f3 (*Fig
237 2SC), with *5lo/alox-5* as the most significant hit.
238
239 Together, these analyses revealed that innate immune responses to wound infections can be
240 trained by prior microbial challenge and suggested that, among the many pathways of
241 reprogramming, neutrophil genes associated with cell migration and swarming can be subject
242 to reprogramming.
243
244 **Neutrophil swarming is enhanced through prior training challenge, and these phenotypic**
245 **changes contribute to disease resistance**
246
247 The changes in gene expression patterns in neutrophils upon training suggested that their
248 migratory behaviour is altered. To relate neutrophil swarm patterns with disease outcome, we
249 combined early imaging of wound infections (0-2 hours post infection-hpi) with monitoring of
250 disease outcome over a longer timescale (up to 24 hpi) in the same larvae **(Fig. 3A)**. We
251 confirmed that in this laser-wound assay, PBS pre-challenged, control fish were more
252 susceptible to PAO1 infection than *E. coli* pre-challenged fish **(Fig. S3A)**. We then compared
253 the behaviour of neutrophils upon wounding and found that in PBS-pre-challenged, control
254 animals, neutrophils exhibited both small-scale clustering and large-scale clustering **(Fig. 3B,**
255 **Movie S2)**. By contrast, in *E. coli*-pre-challenged animals, we observed a more consistent scale
256 of clustering **(Fig. 3B, Movie S2)**. To understand differences in migratory behaviour, we
257 plotted the average neutrophil radial speed (Fig. 3C) and speed (Fig. S3B) over time in PBS
258 versus *E. coli*-pre-challenged fish. *E. coli*-pre-challenged fish showed enhanced migration
259 speeds towards the wound after the first wave of recruitment (1-2 hpi)(Fig. 3C and S3B).
260
261 To relate this variation in swarm kinetics to disease outcome, we plotted the average radial
262 speed per embryo at 1-2 hpi against the bacterial burden outcome measured from the same
263 larva at 24hpi (Fig 3.D). We stratified fish into four categories: i) weak neutrophil recruiters
264 with high bacterial burden (Group 1, G1, in **Fig. 3D**), ii) strong recruiters with high bacterial
265 burden (Group 2, G2, in **Fig. 3D**), iii) strong recruiters with weak bacterial burden (Group 3.
266 G3, in **Fig. 3D**) and iv) weak recruiters with weak bacterial burden (Group 4, G4, in **Fig. 3D**).
267 We considered as 'strong recruiters' those larvae in which the radial speed was above the
268 average radial speed across all larvae. We considered as 'high burden' all the cases above the
269 lowest level of CFU count at which disease symptoms (i.e. disease score more than 1, as per

270 table in Fig. 1B) were observed across all experiments with these two groups of larvae. The
271 number of larvae within G4 did not differ between PBS and *E. coli*-pre-challenged fish, and
272 we reason this group may represent larvae in which bacterial colonisation was weak, as there
273 was neither evidence for neutrophil recruitment nor bacterial burden. Most notably, we found
274 that upon *E. coli* training there was a significant increase of larvae in G3 and a decrease in G1
275 **(Fig. 3E)**.
276
277 As an additional analysis, we measured the maximal rate of neutrophil recruitment across the
278 2 h imaging window. Here, we plotted the number of new neutrophils arriving at the wound
279 over time and determined the slope of the curve during the phase of maximal recruitment **(Fig.**
280 **S3C)**. We then plotted the maximal rate of recruitment against the bacterial burden for the same
281 embryo. We performed similar stratification of larvae in four groups, considering 'fast
282 recruiters' and 'slow recruiters' as those that had a maximal rate of recruitment of either above
283 or below the mean maximal rate, respectively, across all larvae in both PBS and *E. coli*-pre-
284 challenge groups. This analysis indicated a trend for a higher probability of larvae to show fast
285 maximal rate of recruitment and low bacterial burden **(Fig. S3D)**, although the difference was
286 not found to be significant with this sample size **(Fig. S3E)**.
287
288 To measure differences in scale of recruitment, we plotted the number of cells at 2 hpi versus
289 the bacterial burden at 24 hpi in individual larvae. We confirmed that the initial number of
290 neutrophils in the field of view in PBS versus *E. coli*-pre-challenged fish was not significantly
291 different **(Fig. S3F)**. We stratified fish larvae in the same four groups and considered as 'strong
292 recruiters' those larvae in which the cell number exceeded 10 neutrophils. This was based on
293 the distribution of the numbers seen in our experiments and on previous papers indicating a
294 minimal number of clustering neutrophils to correlate with swarming kinetics of
295 recruitment[16,17,54]. We found that upon *E. coli* training there was a significant increase of larvae
296 in G3 and a decrease in G1 **(Fig. 3D)**.
297
298 The tracking analyses suggested that in a proportion of control larvae, the swarm potential of
299 neutrophils is sub-maximal and limits resistance to infection, whereas in *E. coli*-trained larvae,
300 the swarm potential is maximised across different animals. To investigate whether a change in
301 neutrophil swarm potential contributes to wound infection resistance, we used a specific
302 inhibitor for 5-lipoxygenese (5-LO), zileuton, to target the production of the swarm-driving
303 chemoattractant, LTB4. When fish were wounded and infected in the presence of zileuton, the

304 *E. coli*-pre-challenged fish did not show as marked an increase of infection resistance (over
305 PBS-pre-challenged fish), in comparison to when control vehicle (DMSO) was used **(Fig. 3J-**
306 **K)**.
307
308 Together, these results indicated that innate immune training leads to changes in neutrophil
309 swarm patterns upon secondary pathogenic challenge, which in turn influence the probability
310 to resolve infection successfully.
311
312 **5-lipoxygenase enhancement in neutrophils is sufficient to enhance neutrophil swarming**
313 **and resistance from wound infection**
314
315 To determine whether reprogramming of neutrophil swarming is sufficient to influence wound
316 infections, we used genetic engineering of 5-LO in neutrophils. We hypothesised that
317 neutrophils expressing maximal levels of 5-LO would have enhanced swarming capacity and
318 that this may contribute to containment of infection. We first compared the resistance to
319 mechanical wound infection in transgenic larvae in which neutrophils overexpress 5-LO ('5-
320 LO-Neu'; for 5-lipoxygenase overexpressing neutrophils) versus control wild type larvae. We
321 found that 5-LO-Neu larvae showed enhanced resistance to infection, as measured by an
322 improvement in survival rates, disease score and bacterial burden **(Fig. 4A-C)**.
323
324 To relate neutrophil swarm patterns to disease susceptibility, we combined again live imaging
325 during the early stage of wound infection, with subsequent monitoring of disease progression
326 in individual larvae. As with our mechanical wound model, we found that the 5-LO-Neu larvae
327 showed greater resistance to infection in our laser wound infection model **(Fig. S4A and B)**.
328 By observation of the movies, we noted heterogeneity in swarm magnitude across control
329 larvae, which appeared to be less pronounced in 5-LO-Neu larvae **(Fig. 4D** and **Movie S3**).
330 This was not explained by developmental differences in the number of the cells, as the number
331 of neutrophils in the field of view at the start of the movies was comparable **(Fig. S4C)**. To
332 quantify these differences, we first measured neutrophil speed (Fig. S4D) and radial speed (Fig.
333 4E) over time and found that in 5-LO-Neu, neutrophils were faster particularly in the first 1h
334 of observation. We then plotted bacterial burden per larva against radial speed (Fig 4F),
335 maximal rate of recruitment and number of cells recruited (Fig. S4E-H). Accordingly, we
336 stratified fish into four groups: i) weak or slow neutrophil recruiters with high bacterial burden
337 (Group 1, G1, in **Fig S4E, S4G** and **Fig. 4F**), ii) strong or fast recruiters with high bacterial

338 burden (Group 2, G2, in **Fig S4E, S4G** and **Fig. 4F**), iii) strong or fast recruiters with weak
339 bacterial burden (Group 3. G3, in **Fig S4E, S4G** and **Fig. 4F**) and iv) weak or slow recruiters
340 with weak bacterial burden (Group 4, G4, in **Fig S4E, S4G** and **Fig. 4F**). We found that in
341 control larvae, the main outcomes were in groups G1 and G2 whereas in 5-LO-Neu larvae there
342 was increased proportion of outcomes in group G3 and a decrease in group G1. Similar trends
343 were observed whether we used radial speed, number of cells recruited or the maximal rate of
344 recruitment **(Fig. 4G, S4F, S4H)**, except the results using number of cells did not reach
345 significance **(Fig. S4H)**. Together these results suggested that 5-LO enhancement in
346 neutrophils is sufficient to enhance neutrophil swarming rates and that this can provide a
347 beneficial outcome in a subset of larvae.
348
349 Excess neutrophil recruitment can be detrimental for resolution of inflammation and tissue
350 homeostasis. We therefore interrogated whether enhanced neutrophil 5-LO expression could
351 compromise tissue repair and regeneration. To test this, we measured tissue regeneration over
352 2 days post sterile wound injury. We found that 5-LO enhanced animals did not have impaired
353 regeneration and rather showed a trend for improved regeneration. Thus the reprogramming of
354 5-LO in neutrophils did not appear to have a specific physiological counter effect in wound
355 responses.
356
357 **Distinct models of reprogramming swarming during training versus via genetic**
358 **engineering**
359
360 Both natural reprogramming of neutrophils through training and targeted genetic engineering
361 enhanced swarming in a manner that benefited wound defence. However, the phenotypic
362 changes in swarming were distinct in the two cases, with a delayed enhancement of swarming
363 in trained animals (after 1hpi), versus an early enhancement of swarming in 5-LO-engineered
364 animals (before 1hpi). To understand differences in the mechanistic basis of reprogramming,
365 we employed mathematical modelling.
366
367 We modelled the dynamics of the swarming using the simplest model that contains essential
368 chemotaxis and signalling properties that are known for these cells (for the model equations
369 see Materials and Methods section). The chemotaxis of each neutrophil is simply described to
370 arise due to the difference in chemoattractant concentration on opposite sides of the cell, with
371 respect to the source at the wound (Fig. 5A). The chemoattractant triggers a local signal at the

cell edge, which induces cytoskeleton-driven traction forces, with the net chemotactic migration speed given by the difference between these forces at either end of the cell. As the local cellular signal in this model includes the effects of saturation, cells respond weakly both to very weak gradients, and in the presence of large concentrations[55,56]. We focus here on the long time-scale swarming behaviour. Previous work indicated neutrophils mutually stimulate each other to secrete attractant at the wound as they cluster[9]. We therefore assume the chemotaxis be dominated by the chemokine signal that is secreted at the wound by neutrophils, as well as the primary tissue damage signals. In addition to core secretion of attractants by clustering neutrophils, attractants can be further relayed in a wave-like fashion beyond the wound focus[1,10]. When we allow attractant secretion by cells outside the wound we encounter detrimental clustering of cells outside the wound (Fig.S5A and B). This suggests that the relay dynamics may require more complex assumptions to be incorporated in our model. Since the core secretion by neutrophils at the wound was sufficient to reproduce the basic pattern of kinetics of neutrophil swarming (Fig 5B-D), we focused on this reductionist model for our questions here.

Our model assumes that neutrophils arriving at the wound begin to secrete chemokine, thereby increasing its amplitude at the wound, which diffuses and decays outside the wound. Within this model the migration speed of the immune cells towards the wound decreases at high levels of chemokine concentrations, through receptor saturation, which limits their swarming as has been observed experimentally[23].The model includes two additional processes that occur at the wound: First, they can spontaneously switch from secretion of chemokine to producing an active “stop-signal”, which acts to switch cells from secreting the chemokine signal. This was implemented to simulate the rapid arrest of swarming in experimental sterile wounds (Fig.S5C), which did not emerge by receptor saturation alone. Various pathways reported in the literature could play the role of active stop signals[10,24,57]. Secondly, in the presence of bacteria we assume neutrophils sense the bacteria and transition to engaging and attacking the invaders. These attacking neutrophils are assumed to stop secreting the chemokine (or the stop-signal), and they act to both kill and decrease growth of bacteria.

The model describes the average chemotactic migration of the cells in a circular domain around the wound (Fig.5A), where cells are continuously added at the outer boundary to maintain the initial density there fixed. An example of one such simulation is shown in (Fig. 5B-C, Movie S5), where the initial condition has a random distribution of the immune cells outside the

wound. We plotted the trajectories of the cells arriving at the wound within the first 100min, their number and the number of bacteria (Fig. 5D).

We found that the total number of recruited immune cells and bacterial growth can evolve very differently, merely because of fluctuations in the initial distribution of the immune cells around the wound (Fig. S5D). To understand this source of variability better, we compared events where the final number of recruited neutrophils was comparable, but the bacterial burdens were different (Fig. S5E and F). We found that this variation was due to the differences in the initial number of neutrophils proximal to the wound (Fig. S5G) and this prediction matched experimental observations from representative examples (Fig. 4 and Fig. S5H). Since our simulations have fixed parameters, we reason the only source of noise in our simulations (S5D) is the initial distribution of immune cells. In experimental data, we anticipate further sources of variation to influence the scatter. For example, the number of colonising bacteria is expected to vary, and our simulations predict a wider scatter of bacterial growth, independent of neutrophil recruitment kinetics (Fig. S5I and J).

To explore the role of chemoattractant secretion rates in bacterial clearance, we simulated bacterial burden and neutrophils numbers with varying of α rates. As the secretion activity increases, more immune cells are recruited faster which results in diminished bacteria numbers (Fig 5E). However, this improvement in the reduction of the bacterial number saturates, and beyond a certain point higher values of α diminish neutrophil recruitment and bacterial control (Fig 5E inset). This arises due to faster onset of receptor saturation in high attractant levels (Fig. 5F and G). To compare kinetics of neutrophil swarming in trained versus 5-LO engineered animals, we plotted experimental neutrophil speed towards the wound over time (Fig. 5H). Neutrophils in control fish exhibited a plateau following the initial peak in speed. 5LO cells moved initially significantly faster towards the wound, but converged with speeds in control animals by ~90min. By contrast, in trained fish, neutrophils showed an additional peak in speed at later time, at ~100min. These experimental observations can be explained by our model as follows (Fig. 5I): the 5LO-enhanced neutrophils secrete more chemoattractant compared to control cells, and are simulated in our model as having a larger value of α (Fig.5I). As observed experimentally (Fig. S4G an H), our simulations show larger α accounts for higher number of recruited immune cells and lower bacteria proliferation (Fig. 5E). To explain the behavior of neutrophil in trained fish, we hypothesised that neutrophils in these fish have an increased level

of secretion in response to the presence of bacteria. Here neutrophils have a basal level of secretion strength α_0, which can be further increased in response to bacteria presence (Eq.11 in Material and Methods). This combination of higher sensitivity to bacteria and increased secretion rates recapitulated observed kinetics of delayed enhancement of neutrophil swarming in trained fish (Fig.5I). Note that in our model there is persistent recruitment over long periods in the presence of bacteria (Fig.5I), as opposed to very brief transient recruitment in sterile wounds (Fig.S5C), as observed in experiments. This behavior emerges in our model simply due to the weak stop-signal as cells in the wound continuously switch from secretion to engaging with the bacteria.

Together, this evidence showed that i) core secretion by neutrophils at the wound along with stop signals describe the basic swarm kinetics of neutrophils and that ii) distinct swarm reprogramming mechanisms can achieve improvement in bacterial clearance.

Discussion

Here, we examine whether self-generated guidance is a programmable process and the extent to which such reprogramming can affect disease outcome. We show that neutrophil swarming and the expression of genes for swarm machinery are altered during natural reprogramming ('training') by microbial experience. Through chemical inhibition, we found that these alterations contribute to enhanced resistance of trained animals to pathogenic infection. Through quantitative live imaging and modelling, we demonstrate how variations in secretion of chemoattractant by neutrophils lead to changes in swarm kinetics, bacterial clearance and infection outcome. Finally, we show that enhancing the ability of neutrophils to produce autologous chemoattractants (through 5-LO engineering) is sufficient to accelerate neutrophil swarming and improve bacterial clearance and disease progression.

Whilst exploring tissue variables influencing bacterial wound infection, we found that osmotic surveillance during tissue damage plays a major role in resistance to opportunistic wound infection. This extends findings reported previously, using *P. aeruginosa* microinjection in the context of wound infection[49]. Previous studies conversely reported that damage detection through osmotic surveillance compromised *Candida albicans* wound infection outcome[58]. Mechanistically, this was attributed to keratinocyte movement in response to hypotonic

472 medium detection, which, rather than limiting microbial colonisation, appeared to favour tissue
473 spreading of *C. albicans*. These discrepancies suggest that the role of osmotic surveillance in
474 wound infection outcome depends on the type of invading microbe. For example, *P. aeruginosa*
475 bacteria are highly mobile[59] and thus may rely less on host tissue movements for spreading
476 than *C. albicans*.
477
478 Our study highlights novel routes for training in wound infection settings. We observed
479 improved resistance to bacterial wound infection after a pre-challenge with non-pathogenic *E.*
480 *coli*. Probiotic *E. coli* strains have been reported to have beneficial effects on viral resistance
481 in mouse models[60], but such training has not been reported for wound infection. Neutrophil
482 training in zebrafish larvae arises through changes in hematopoietic stem cells within similar
483 timeframes post-infection, as has been reported in adult mammals[36]. Our observations are
484 consistent with central reprogramming of neutrophils, as the protective effects were seen across
485 heterologous tissue sites and the gene expression changes were detectable in neutrophils
486 isolated from hematopoietic tissue. In addition, we showed that zebrafish neutrophils undergo
487 epigenetic modifications on swarm-associated genes during training with *Shigella flexneri*
488 (which are phylogenetically close to *E. coli)* in a comparable timeframe with our study[38].
489
490 We found that neutrophil swarm capacity is amenable to reprogramming after microbial
491 experience. Specifically, neutrophils upregulated expression of genes associated with
492 swarming and trained larvae were less likely to show poor swarming and high susceptibility to
493 infection. This suggests that training primarily benefits subgroups of larvae with submaximal
494 swarming. Inter-individual variation in training has notably been reported in humans exposed
495 to Bacillus Calmette-Guérin (BCG) vaccine, wherein training improved outcome in a
496 subpopulation of individuals with sub-maximal immunological profiles at the time of
497 vaccination[61]. Interestingly, we found that training also reduced the higher-end values for
498 swarm kinetics (with migration kinetics more closely clustered around a medium range). One
499 potential explanation is that the effect of increasing neutrophil numbers has non-linear effects
500 on bacterial clearance, whereby at low neutrophil numbers the changes in neutrophil kinetics
501 can make a significant difference in bacterial clearance whereas beyond a certain number of
502 recruited neutrophils, the benefit decreases. Our mathematical modelling supports this model
503 and suggested that beyond a certain point, increasing the secretion of chemoattactant has no
504 benefit for bacterial clearance and can even be detrimental to clearance. A question raised is
505 why neutrophil swarming has not evolved to be maximal at steady state. In our model,

enhanced swarming did not delay regeneration, suggesting that there is no detriment to physiological wound repair processes. We therefore speculate that adaptive reprogramming of neutrophil swarming may reflect a strategy to economise energy or a means to balance the risks of overt inflammation in chronic inflammatory settings.

We used mathematical modelling to understand how different dynamics of chemoattractant secretion can influence neutrophil swarm kinetics and bacterial clearance. Our experimental data indicated distinct kinetics of swarm enhancement in trained animals versus 5-LO engineered animals, wih a delayed peak of swarming in the former and an early peak in the latter. A general explanation is that in trained animals a range of genes are altered whereas in 5-LO engineered animals, the enhancement is specific to chemoattractant secretion. We explored theoretical parameters that could be altered during training. Our mathematical model predicts that a combination of upregulation of swarm machinery (e.g. 5-LO expression) together with enhanced sensitivity to bacterial detection and bacteria-dependent secretion can produce the delayed swarm peak seen in trained fish. This theory aligns with evidence from the literature, in that LTB4 secretion is triggered by bacterial detection through Toll like receptor (TLR) signalling[62] and that TLR signalling pathways can be reprogrammed during trained immunity[28]. It is noteworthy that epigenetic H3K4 marks were detected along the catabolic regulator of LTB4 *cyp4f3*, suggesting that training may fine tune LTB4 dynamics in a more complex manner. Future studies could aim to dissect these circuits and recapitulate these by genetic engineering.

Our discovery that engineering 5-LO is sufficient to improve bacterial clearance has relevance to cellular immunotherapies. Strategies for genetic modification of immune cells are growing and extending to cell types beyond lymphocytes, due to advances in genetic engineering and stem cell biology[40,41,43,63]. In this backdrop, the engineering of chemoattractant receptors has been conceptualised to improve the efficacy of CAR-engineered immune cell deployment to tumors[64]. Our study suggests that harnessing the ability of immune cells to seed chemoattractant gradients in target tissues may offer new routes for reprogramming immune cell migratory patterns.

Acknowledgements

The *P. aeruginosa* strain was kindly provided by Prof. Martin Welch, Department of Biochemistry, University of Cambridge and the *E. coli* strain was kindly provided by Dr. Somenath Bakshi, Department of Engineering, University of Cambridge. We thank Margarida C. Gomes and Serge Mostowy for sharing the ChIP-seq data from trained zebrafish. S.M.B., I.W., G.R., C.C., Y.L. were supported by the European Research Council (ERC) under the Horizon 2020 program and UKRI, Grant agreement No. EP/Y02799X/1. Y.L. is also supported by a BBSRC DTP programme BB/X010899/1. N.S.G. is the incumbent of the Lee and William Abramowitz Professorial Chair of Biophysics (Weizmann Institute) and acknowledges support from the Royal Society Wolfson Visiting Fellowship, and Human Frontier Science Program grant RGP0032/2022. H.A.W. was supported by an MRC DTP studentship (MR/N013433/1) and a Leverhulme Trust grant (RPG-2021-226). H.M.C. was supported by the Roving Researcher scheme in the School of Biological Sciences, University of Cambridge. A.D. was supported by a MIRES scholarship from IdEx Université Paris Cité ANR-18-IDEX-0001, funded by the French Government through its 'Investments for the Future' program. The authors gratefully acknowledge the Cambridge Imaging Centre for their support and assistance in this work.

Competing Interests

The authors declare no competing interests

Code availability

The available codes used for modelling neutrophil swarming can be found here:
https://github.com/samantatuhin1991/immune-swarming-model

Methods

Experimental model and subject details

All zebrafish were maintained in accordance with UK Home Office regulations under the UK Animals (Scientific Procedures) Act 1986 (PPL number PP4458156), with approval from the University Biomedical Service Committee. Adult fish were maintained and bred following established protocols[65]. Briefly, zebrafish were bred and maintained under standard conditions at 28.5 ± 0.5 °C on a 14 h light:10 h dark cycle. Embryos were collected from natural spawnings at 3 hours post-fertilization (hpf), bleached for 5 minutes in 0.003% sodium hypochlorite (NaOCl; Cleanline, CL3013), and rinsed three times with E3 medium. They were subsequently incubated at 28 °C in E3 medium supplemented with 0.1 µg /ml methylene blue (Sigma-Aldrich, M9140-25G). For imaging experiments, E3 medium was additionally supplemented with 0.003% 1-phenyl-2-thiourea (PTU; Sigma Aldrich, P7629) to inhibit pigmentation and preserve optical transparency.

For experiments that required *E. coli* training, *E. coli* was administered to larvae at 2 days post-fertilization (dpf) and subsequent re-challenge experiments were done at the 4 dpf stage. In experiments without training, larvae at 3-4 dpf were used. For live imaging, larvae were anesthetized in appropriate buffer containing 160-200 mg/L MS-222 (Sigma-Aldrich, E10521-50G). Where indicated, larvae were treated with Zileuton (20 µM, Tocris, 3308) or appropriate volume of vehicle (DMSO (Sigma-Aldrich, 276855-100ML)) solution by immersion.

The following transgenic zebrafish lines were used: Tg(*lyz*:GCamp6F)^{cu104} and Tg(*lyz:*tRFP-5LO) ^{cu106} from previously described work[9] ,Tg(*mpx*:GFP)i114[66], Tg(*runx1+23*:mCherry).

Bacterial culture and preparation

For *E. coli* injection, cyan fluorescent protein (CFP)-expressing *E. coli* MG1655 7740 strain was developed as described previously[67]. A single colony was obtained from a four-way streak on antibiotic-free LB Agar (Melford, A20020-500.0) plate. The colony was inoculated into 50 ml of antibiotic-free LB broth (Formedium, LBX0102) and cultured at 37 °C with shaking until the OD_{600} reading reached 0.8-0.9. The culture was then aliquoted into 1 ml stocks in antibiotic-free LB broth with 20% v/v glycerol (Fisher Scientific, G/0650/17), snap-frozen with liquid nitrogen, and stored at -80 °C until usage. On the day of the experiment, aliquots of *E. coli* were thawed at 37 °C, pelleted by centrifugation at 5,000 × *g* for seven minutes at 4 °C, and

599 washed twice with PBS (Sigma Aldrich, D8537). The bacteria were finally suspended in PBS
600 with 10% v/v phenol red (Sigma, P0290).
601 For *P. aeruginosa* infection, PAO1 strain was used[9]. One day prior to infection, a single colony
602 of *P. aeruginosa* was obtained from a four-way streak on Pseudomonas Isolation Agar (PIA;
603 BD Difco, 292710) supplemented with cetrimide and nalidixic acid (E&O Laboratories Ltd,
604 LS0006) and glycerol. The colony was inoculated into 5 ml of antibiotic-free LB broth and
605 cultured at 37 °C with shaking for 24 h. On the day of the experiment, the overnight culture
606 was diluted in fresh LB and incubated to mid-logarithmic phase (OD_{600} = 0.6–0.8). Bacterial
607 density was adjusted to 3×10^5 CFU/mL using spectrophotometric estimation. Bacteria were
608 pelleted at 1700 × *g* for five minutes and washed twice with PBS to remove residual growth
609 medium, then resuspended in PBS.
610
611 **PBS and *E. coli* injections**
612 On the day of injections, *E. coli* injection mix was prepared as described above. PBS injection
613 mix was prepared as PBS with 10% v/v phenol red for control. Larvae were anaesthetised in
614 E3 medium supplemented with 0.1 µg/ml methylene blue and 160-200mg/L MS-222. The left
615 otic vesicle of each zebrafish larva was then injected with 2 drops of 0.125 nL of PBS or *E.*
616 *coli* injection mix with a pressure of 20 psi using Picospritzer III microinjector (Intracell), as
617 previously described[68]. To confirm the dose of *E. coli* injected, 2 drops of 0.125 nL of injection
618 mix was directly injected into a microcentrifuge tube containing 100 µl PBS after the injections
619 and were then plated onto antibiotic-free LB Agar plates overnight at 37 °C at 10^0 and 10^{-1}
620 dilution. The bacterial colony forming units (CFU) were then determined by counting the
621 number of CFP^+ colonies after overnight incubation. Only when the *E. coli* injection dose
622 exceeded 400 CFU/ml were the larvae included for subsequent experiments. After injections,
623 larvae were transferred to fresh E3 medium supplemented with 0.1 µg/mL methylene blue and
624 kept at 28 °C until further use.
625
626 **Tail transection, wound infection and survival assay**
627
628 Zebrafish larvae were transferred to a Petri dish containing Ringer's solution and 160-200 mg/L
629 MS-222. Tail transection was done using a surgical blade (Swann Morton, 0510) at the distal
630 boundary of the notochord, avoiding injury to the notochord. Non-transected larvae served as
631 controls. Immediately after tail transection, larvae were transferred to a six-well plate
632 containing Ringer's solution with 3×10^5 CFU/mL *P. aeruginosa* (for the role of specific

633 buffers, E3/isotonic E3/Ringer were used as indicated) and incubated at 32 °C for 3 h. After
634 incubation, larvae were washed five times in E3 medium (without methylene blue). Individual
635 larvae were then placed in wells of a 24-well plate containing 1 mL E3 (without methylene
636 blue) and monitored for survival and disease progression. For 5-LO inhibition assays, 20 μM
637 zileuton treatment (diluted in DMSO) was initiated 1 h prior to tail transection and maintained
638 until the end of the experiment.
639
640 Survival was assessed immediately after washing, at 3 hpi, and 24 hpi. Assessment was also
641 done at intermediate time points (7 hpi and 10 hpi) when experiment was done for 24 h. For
642 48h time point experiments, analysis was done at 3 h, 24 h and 48 h. Phenotypic disease scoring
643 was based on behavioural responses, transparency, tissue integrity, circulation, and survival.
644 Between observation timepoints, larvae were returned to 32 °C. A score of 4 was defined as
645 death of the organism that was determined by the absence of heartbeat as observed under the
646 microscope.
647
648 **Measurement of regeneration after sterile tail transection**
649
650 Caudal fin transection of zebrafish larvae (3dpf) was performed using a sterile surgical blade
651 at the boundary of the notochord, without injuring the notochord. Following injury, larvae were
652 rinsed with E3 medium and placed in individual wells of a 24-well plate in E3 medium, at
653 28.5°C. Images of each larva was acquired on a stereomicroscope (Zeiss Stemi 2000-C)
654 immediately after caudal fin transection (0h), one day after transection (24h) and two days after
655 transection (48 h).

656 For every larva, the caudal fin area posterior to the notochord was outlined using the Freehand
657 selection tool in ImageJ/Fiji for images acquired at all the three time points. The outlined area
658 was measured to obtain a total surface area of the region of interest (ROI). The area of the ROI
659 at 24 h and 48 h for each larva was normalized by the area of the ROI for the same larva at 0
660 h.

661 **Bacterial burden quantification**
662 At indicated timepoints, zebrafish larvae from each condition were pooled into groups of three
663 larvae and homogenised in 300 μL PBS containing 0.1% v/v Triton X-100 (VWR, 28817.295)
664 using sterile pestles. Serial dilutions (up to 10^{-3}) were prepared in PBS and plated on PIA
665 supplemented with cetrimide and nalidixic acid (as per manufacturer's instructions) for *P.*

666 *aeruginosa* or antibiotic-free LB agar for *E. coli.* CFU were then counted after 24 hours
667 incubation.
668
669 **Fluorescence-Activated Cell Sorting (FACS)**
670 Approximately 400 embryos from a cross between Tg(*mpx*:GFP)^{i114} and
671 Tg(*runx1+23*:mCherry) transgenic lines were injected with either *E. coli* or PBS (200 per
672 group) in the otic vesicles at 2 dpf as described above. At 4 dpf, larvae were collected into
673 microcentrifuge tubes, rinsed twice with 1x HBSS (prepared by diluting 10x HBSS (Gibco™,
674 14175095) in UltraPure™ DNase/RNase-Free Distilled Water (Invitrogen™, 10977035)), and
675 placed on ice for 10 minutes to immobilise the larvae. The caudal haematopoietic tissue (CHT)
676 regions from the larvae were dissected on sterile petri dishes using ethanol-sterilised scalpels
677 and centrifuged to remove excess HBSS.
678 For tissue dissociation, 500 µL of digestion solution (2% w/v collagenase (Gibco™, 17104019)
679 and 40% v/v trypsin (Gibco™, 15400054) in 1x HBSS) was added to each tube. Samples were
680 incubated at 30 °C for 30 minutes with periodic trituration by pipetting. Digestion was halted
681 with 1x HBSS containing 10% v/v heat-inactivated fetal bovine serum (FBS; Gibco™,
682 A5670701). All subsequent steps were performed on ice. Cells were centrifuged at 500 × g for
683 5 minutes at 4 °C and then resuspended in sorting solution (1x HBSS supplemented with 10
684 mM HEPES 15630056) and 2% FBS) and filtered through a pre-wetted 40 µm cell strainer
685 (Falcon, 352340). Filtered cells were centrifuged and resuspended in 1 ml sorting solution in a
686 microcentrifuge tube. Cell viability and concentration were assessed using trypan blue (Gibco,
687 15250) staining and a hemocytometer, respectively.
688 GFP-positive neutrophils were FAC-sorted using a BD FACS Aria III (Becton Dickinson)
689 directly into 100 µL of lysis solution supplied with the RNAqueous® Micro Kit (ThermoFisher,
690 AM1931).
691
692 **RNA extraction and cDNA synthesis**
693 For transcriptomic analysis, RNA isolation was done from the sorted cells using the
694 RNAqueous® Micro Kit (Thermo Fisher, AM1931) according to the manufacturer's
695 instructions, including DNase I digestion step to eliminate genomic DNA contamination.
696
697 For cytokine expression analysis following PBS/ *E. coli* injections, at 2 dpf, RNA was extracted
698 from groups of 10 wild-type zebrafish per condition (non-injected, PBS-injected, and *E. coli*-
699 injected) after euthanasia with MS-222 at 4.5 hours post-injection using the RNeasy® Mini Kit

700 (Qiagen, 74104). Subsequently, from 3 to 10 dpf, groups of 8-10 larvae per condition were
701 euthanised with MS-222 prior to RNA extraction.
702
703 The obtained RNA concentrations were measured using the Nanodrop. Purified RNA was then
704 reverse transcribed into cDNA using the Maxima H Minus First Strand cDNA Synthesis Kit
705 (ThermoFisher, K1651) following the manufacturer's protocol. Finally, cDNA was stored at -
706 20 °C until further use for quantitative PCR (qPCR) analysis.
707
708 **Gene expression analysis**
709
710 The qRT-PCR was performed using the PowerTrackTM SYBR™ Green Master Mix
711 (ThermoFisher, A46012) and carried out in the LightCycler® 480 Instrument II (Roche). For
712 transcriptomic analysis, each reaction contained 0.5 ng of cDNA, 10 nM of primer pairs, and
713 1X master mix. The zebrafish gene *rpl32* served as the reference for normalisation.
714 For cytokine expression analysis, each reaction contained 5 ng cDNA, 500 nM primer pairs,
715 and 1X master mix and the zebrafish gene *ef1a* served as the reference for normalisation.
716 The mRNA levels of target genes relative to a housekeeping gene (**Table 1)** were calculated
717 using the Livak ($2^{-\Delta\Delta Cqt}$) method[69]. All qRT-PCR reactions for transcriptomic analysis were
718 performed in duplicate with five biological repeats for transcriptomic analysis while the
719 cytokine expression experiments were performed in triplicate with three biological repeats.
720
721 **Table 1**
722

Gene	**Primer Sequences (5′ → 3′)**
5-lo	Forward: GAGATGGCAGGGCTCGATTG Reverse: TACTCATCGGGAAGCCAGGA
cx43	Forward: GCTCTCCACTCTTTACTTCTTTCCAG Reverse: GTATTGCACTTGAAAGCTGACTGC
cxcl8a	Forward: GTCGCTGCATTGAAACAGAA Reverse: CTTAACCCATGGAGCAGAGG
cxcl8b	Forward: CTACCGAGACGTGGGTGATT Reverse: GCTCGGTGAATGGTCATTTT
cxcr2	Forward: TGACCTGCTTTTTTCCCTCACT

	Reverse: TGACCGGCGTGGAGGTA
cxcr1	Forward: GTGATCGTACGCGCTATGGA Reverse: ATTCGGGTTGCTAATCGCCA
tubg1	Forward: GGATACACACCGCTGACCAC Reverse: AGCCTCCTCATCACATCCAGA
rpl32	Forward: CCCTCACCAAACCTAAGATCGT Reverse: CTCCAGTTTGCCCTGATCTTG
ef1a (housekeeping)	Forward: AAGGAGAAGATCGACCGTCG Reverse: TGATTGAGGGAAATTCACTTGG
cxcl18b	Forward: TGCCAGTGTGAAGAGTCATC Reverse: TCGCAGTTTGGTCTTTTAGGG
il6	Forward: AGACGAGCAGTTTGAGAGAGATT Reverse: GTTTGAGGAGAGGAGTGCTGAT
il1b	Forward: ATCAAACCCCAATCCACAGAGT Reverse: GGCACTGAATCCACCACGTT

ChIP-seq Data Analysis and Visualisation

H3K4me3 ChIP-seq data from *Shigella*-trained zebrafish neutrophils were obtained from GEO accession GSE217063[38].Processed peak files were filtered to extract signal values and q-values for promoter regions (≤1 kb from transcription start site) of five swarming-associated genes (*cyp4f3, lta4h, alox5a, pla2g4aa, alox5ap*). Heatmaps were generated using the pheatmap package in R, with statistical significance ($q < 0.05$) indicated by asterisks. Permission for data use was obtained from the corresponding author of the original study.

Two-photon imaging and laser wounding

Two photon imaging was performed in Tg(*lyz*:GCaMP6f)^{cu104} larvae or larvae from crosses between Tg(*lyz*:GCaMP6f) x Tg(*lyz:*tRFP-5LO). Transgenic larvae expressing the calcium indicator GCaMP6f were screened to ensure high reporter expression. Larvae exhibiting strong fluorescence and normal morphology were selected for imaging and infection. Selected larvae were anaesthetised and mounted in a mixture of 1.2% low-melting-point agarose (Invitrogen, 16520) and the medium (E3, isotonic E3, Ringer) containing 160-200 mg/L MS-222. Imaging under sterile conditions was performed as as previously described[50]. For sterile imaging, larvae were mounted on a 35 mm glass-bottom dish with a 14 mm microwell #1.5 coverglass. Excess

741 agarose was removed before solidification to embed the larvae in a thin layer. For infection
742 imaging, larvae were mounted in a custom-built coverslip chamber consisting of glass
743 coverslips sealing both the top and bottom of the sample onto a metallic ring. Larvae were
744 oriented laterally, and the agarose was allowed to solidify. After agarose solidification, the
745 urogenital region was exposed by carefully removing surrounding agarose under a dissecting
746 microscope using a pair of forceps, allowing bacterial access post-wounding. The chamber (for
747 infection conditions) or dishes (for sterile conditions) were filled with 1 mL or 4 mL of Ringer's
748 solution containing 160-200 mg/L MS-222 and 3×10^5 CFU/mL PAO1. For sterile conditions,
749 appropriate buffer (Ringer/ E3 or isotonic E3) was used as indicated.
750 Laser ablation and time-lapse imaging were performed on a LaVision TriM Scope multiphoton
751 microscope equipped with an electro-optic modulator for rapid power modulation. A Spectra-
752 Physics Insight DeepSee dual-line laser was tuned to 900 nm for imaging and 1,040 nm for
753 ablation, with imaging power set to ~500 mW at the specimen plane. Image acquisition was
754 controlled using ImSpector Pro software (version 5.0.284.0; LaVision Biotec, ©1998–2016).
755 Two-photon imaging was conducted with a 25×/NA 1.05 water-dipping objective. A 40 µm-
756 diameter region of interest was defined on a single superficial focal plane (240 nm/pixel, 15 µs
757 dwell time). Z-stacks (~20 planes, 2 µm step size) were acquired every 20 s. Laser wounding
758 was initiated after a 2 min pre-wound baseline, followed by 2 h of post-wound imaging. Focus
759 was maintained throughout acquisition. Image stacks were processed in Fiji using maximum-
760 intensity z-projections to generate neutrophil-swarming time-lapse movies for subsequent
761 analysis.
762
763 **Image analyses**
764 ***Defining the cumulative number of cells arriving at the wound***
765 The cumulative number of neutrophils that reach the wound were calculated by manually
766 counting the neutrophils reaching the wound in blinded datasets using ImageJ/Fiji overtime.
767
768 ***Cell trajectories speed and radial speed***
769 Neutrophils were semi-automatically tracked using Imaris v8.2 (Bitplane AG, Zürich,
770 Switzerland) on 2D maximum intensity projections of the 4D time-lapse movies. Speed and
771 cell position data of the tracked cells overtime from Imaris were exported using Excel 2016.
772 Radial speed was calculated using MATLAB scripts developed previously[9]. Briefly, for
773 normalised radial speed calculations, instantaneous speed values for individual neutrophils
774 were divided by the mean instantaneous speed value of the corresponding embryo and

775 multiplied for the cosine of the angle. Tissue drift was observed in the first 20 minutes after
776 LW, therefore, these timepoints were excluded from speed and radial speed analyses. Movies
777 in which there was considerable tissue drift throughout the imaging window or where the
778 wound was too small to cause any detectable response were excluded from the analysis.
779
780 ***Defining maximum rate of recruitment***
781 After image acquisition, each movie was manually analysed using Fiji, to determine the number
782 of cells recruited to the wound overtime. Using the number of cells recruited at set time points
783 (at 0 min, 5 min and then every 15 min), the maximum rate of recruitment's function was
784 calculated. In this, only the active recruitment timepoints were considered (i.e. if the
785 recruitment started at 15 min, the timepoints 0 and 5 min were not considered. Similarly, if the
786 recruitment of cells plateaued at later timepoints, those timepoints were not considered for the
787 calculation).
788
789 ***Measuring rate of wound closure***
790
791 Time-lapse movies of laser wounding in zebrafish larvae (3dpf) in three buffers (E3, isotonic
792 E3 and Ringer) were acquired as mentioned above. All movies were blinded before analysis of
793 wound closure. Each time lapse movie was opened using ImageJ/Fiji. The first slice in which
794 the impact of the wound is visible is noted. For analysis of the wound closure, the slice after
795 the first visible impact of the wound is selected as the time of wound (t=0 mins). Using the
796 freehand selection tool, the margin of the wound is selected as the region of interest (ROI) and
797 the area of the ROI measured. Similarly, the wound region is outlined in all subsequent time
798 points, and their corresponding area of ROI is measured (until t=20 mins). Exporting the area
799 onto an excel sheet, the area at each time point is normalized by the initial area (t=0). The
800 resulting value is plotted over time. A non-linear regression (curve fit) analysis was done using
801 GraphPad Prism. Briefly, the one phase decay model with the least squares regression method
802 was employed. The comparison was done to check if the best-fit values for the three conditions
803 differ for all parameters (Y0, plateau and K).
804
805 ***Statistical analyses***
806

All statistical tests were performed in Prism10 (GraphPad Software, La Jolla, CA). The statistical test and the n number are indicated in the figure legends. The error bars show standard error of the mean except for bacterial burden data where error bars represent 95% confidence intervals of the median. Where the distribution was verified as normal, outliers were removed by applying Rout test. Live imaging experiments were acquired in minimum five independent experiments. A normal distribution test was performed prior to any *t*-test statistical analyses. Normal distribution was assessed using *Shapiro-Wilk test*.

Theoretical model

The signal triggered by the local concentration of the chemokine ($\mathrm{c(r)}$), at the cell edge is given by (Fig.5(a,b)):

$$\mathrm{s(r)} = \frac{\mathrm{c(r)}}{\mathrm{c(r)+c_s}} \qquad (1)$$

And the net cell speed up the chemokine gradient is given by the difference of the traction forces across the opposite ends of the cell, with respect to the direction of the wound (given by unit vector $\hat{n}$, Fig.5(a,b))

$$\vec{v}(r) = v_0[s(r+R) - s(r-R)]\hat{n} \qquad (2)$$

Where R is the typical cell radius and v_0 its maximal migration speed. We ignore here the random component to the cell speed, so that we focus on the average speed towards the wound due to the chemokine signal.

We focus here on the long-time swarming behavior, which we assume to be dominated by the chemokine signal that is secreted at the wound. We assume that the chemokine concentration has an exponentially profile decaying radially away from the wound, with its amplitude at the wound cite dependent on the number of chemokine secreting neutrophils (n_s). Neutrophils arriving at the wound are assumed to start secreting chemokine, so that the chemokine profile has the form:

$$c(r,t) = \left(c_0 + \alpha n_s(t)\right)\exp\left(-\frac{r}{r_0}\right) \quad (3)$$

The equation for the evolution of the number of chemokine secreting neutrophils at the wound is given by

$$\frac{dn_s(t)}{dt} = J_{wound} - \gamma(t)n_s(t) - k_{\mathrm{to_attack}}(t)\,n_s(t) \qquad (4)$$

Where J_{wound} is the flux of cells arriving at the wound from the migration domain (Fig.Xa). The second and third terms describe the rates at which the chemokine secreting cells change their states to "stop-signal" mode (n_{ss}) and bacteria-attack model (n_b).

The secreting neutrophils undergo a spontaneous transition to a "stop-signal" mode (n_{ss}), at a rate γ. We assume that this rate has a basal value (γ_0), but is dominated by the "stop-signal" secreted by n_{ss} cells, in the form:

$$\gamma(t) = \gamma_0 + \gamma_1 \frac{n_{ss}(t)}{n_{ss}(t)+n_{s,ss}} \qquad (5)$$

Where γ_1 is the parameter describing the "stop-signal" effectiveness, and $n_{s,ss}$ describes the saturation of the response to this signal. The number of "stop-signal" cells evolves according to the following equation

$$\frac{dn_{ss}(t)}{dt} = \gamma n_s(t) - k_{\text{to_attack}}(t)\, n_{ss}(t) \quad (6)$$

Note that while the influx of cells into the wound is discrete, determined by the arrival of the particles migrating to the wound within the simulation domain (Fig.5a), the subsequent evolution of the numbers of cells in each of the states evolve according to continuum equations (Eqs.4,6) for simplicity.

Finally, we consider the dynamics of the invading bacteria and their effect on the neutrophils. The neutrophils are able to sense the presence of bacteria [ref] and this signal, which is proportional to the number of bacteria, triggers the transition of neutrophils from the chemokine and stop-signal secreting states into "attack" mode (n_b), at a rate given by

$$k_{\text{to_attack}}(t) = k_{\text{to_attack},0} \cdot \frac{B(t)}{B(t)+B_{\text{sat}}} \qquad (7)$$

Where $k_{\text{to_attack},0}$ is some constant rate, $B(t)$ is the number of bacteria in the wound at time t and B_{sat} is some saturation constant. The equation of the time evolution of the number of neutrophils in "attack" mode is given by

$$\frac{dn_b(t)}{dt} = k_{\text{to_attack}}(t) \cdot [n_s(t) + n_{ss}(t)] - \beta \cdot \frac{B(t)}{B(t)+B_{\text{sat},1}} \cdot n_b(t) \qquad (8)$$

Where the last term describes the rate at which neutrophils get killed/consumed due to their engagement with the bacteria. This term includes a saturation which describes a maximal number of bacteria that each neutrophil can interact with, of order of the saturation constant $B_{\text{sat},1}$.

The dynamics of the bacteria is given by the following equation

$$\frac{dB(t)}{dt} = k_{\text{grow}}(t) \cdot B(t) - \eta n_b(t) \cdot \frac{B(t)}{B(t)+B_{\text{sat},1}} \quad (9)$$

Where the first term describes their growth rate, given by

$$k_{\text{grow}}(t) = \frac{k_{\text{grow},0}}{1+n_b(t)/N_{\text{att,grow}}} \qquad (10)$$

Where $k_{\text{grow},0}$ is a constant, and we consider that the neutrophils can diminish the bacterial growth rate, as described by the denominator. The last term in Eq.(9) describes the rate at which bacteria are removed/destroyed by the neutrophils.

Finally, we also consider that the secretion of the chemoattractant can be increased in response to the presence of bacteria. We use a form as in Eq.(7), such that

$$\alpha(t) = \alpha_0 + \alpha_1 \cdot \frac{B(t)}{B(t)+B_{\text{s}}} \qquad (11)$$

The list of the model parameters is given in Table I in the Supplmentary Information section.

References

1. Schrope, J. H., Robertson, T. F., Sarris, M. & Huttenlocher, A. Chemical and Mechanical Regulation of Leukocyte Migration. *Cold Spring Harb. Perspect. Biol.* a041752 (2025) doi:10.1101/cshperspect.a041752.
2. Insall, R. H., Paschke, P. & Tweedy, L. Steering yourself by the bootstraps: how cells create their own gradients for chemotaxis. *Trends Cell Biol.* **32**, 585–596 (2022).
3. Stock, J., Kazmar, T., Schlumm, F., Hannezo, E. & Pauli, A. A self-generated Toddler gradient guides mesodermal cell migration. *Sci. Adv.* **8**, eadd2488 (2022).
4. Uçar, M. C., Alsberga, Z., Alanko, J., Sixt, M. & Hannezo, E. Self-generated chemotaxis of mixed cell populations. *Proc. Natl. Acad. Sci.* **122**, e2504064122 (2025).
5. Dalle Nogare, D. & Chitnis, A. B. A framework for understanding morphogenesis and migration of the zebrafish posterior Lateral Line primordium. *Mech. Dev.* **148**, 69–78 (2017).
6. Muinonen-Martin, A. J. *et al.* Melanoma Cells Break Down LPA to Establish Local Gradients That Drive Chemotactic Dispersal. *PLoS Biol.* **12**, e1001966 (2014).
7. Tweedy, L. *et al.* Seeing around corners: Cells solve mazes and respond at a distance using attractant breakdown. *Science* **369**, eaay9792 (2020).
8. Lämmermann, T. *et al.* Neutrophil swarms require LTB4 and integrins at sites of cell death in vivo. *Nature* **498**, 371–375 (2013).
9. Poplimont, H. *et al.* Neutrophil Swarming in Damaged Tissue Is Orchestrated by Connexins and Cooperative Calcium Alarm Signals. *Curr. Biol.* **30**, 2761-2776.e7 (2020).

904 10. Strickland, E. *et al.* Self-extinguishing relay waves enable homeostatic control of
905 human neutrophil swarming. *Dev. Cell* **59**, 2659-2671.e4 (2024).
906 11. Afonso, P. V. *et al.* LTB4 Is a Signal-Relay Molecule during Neutrophil Chemotaxis.
907 *Dev. Cell* **22**, 1079–1091 (2012).
908 12. Alanko, J. *et al.* CCR7 acts as both a sensor and a sink for CCL19 to coordinate
909 collective leukocyte migration. *Sci. Immunol.* **8**, eadc9584 (2023).
910 13. Dowdell, A., Paschke, P. I., Thomason, P. A., Tweedy, L. & Insall, R. H. Competition
911 between chemoattractants causes unexpected complexity and can explain negative
912 chemotaxis. *Curr. Biol.* **33**, 1704-1715.e3 (2023).
913 14. Burn, G. L., Foti, A., Marsman, G., Patel, D. F. & Zychlinsky, A. The Neutrophil.
914 *Immunity* **54**, 1377–1391 (2021).
915 15. Reátegui, E. *et al.* Microscale arrays for the profiling of start and stop signals
916 coordinating human-neutrophil swarming. *Nat. Biomed. Eng.* **1**, 0094 (2017).
917 16. Ng, L. G. *et al.* Visualizing the Neutrophil Response to Sterile Tissue Injury in Mouse
918 Dermis Reveals a Three-Phase Cascade of Events. *J. Invest. Dermatol.* **131**, 2058–
919 2068 (2011).
920 17. Chtanova, T. *et al.* Dynamics of Neutrophil Migration in Lymph Nodes during
921 Infection. *Immunity* **29**, 487–496 (2008).
922 18. Hopke, A. *et al.* Neutrophil swarming delays the growth of clusters of pathogenic
923 fungi. *Nat. Commun.* **11**, 2031 (2020).
924 19. Saraswat, D. *et al.* Neutrophil swarming is crucial for limiting oral mucosal infection
925 by *Candida albicans*. *J. Leukoc. Biol.* **117**, qiae239 (2025).
926 20. Herrero-Cervera, A., Soehnlein, O. & Kenne, E. Neutrophils in chronic inflammatory
927 diseases. *Cell. Mol. Immunol.* **19**, 177–191 (2022).

928 21. Isles, H. M. *et al.* Pioneer neutrophils release chromatin within in vivo swarms. *eLife*
929 **10**, e68755 (2021).
930 22. Khazen, R. *et al.* Spatiotemporal dynamics of calcium signals during neutrophil
931 cluster formation. *Proc. Natl. Acad. Sci.* **119**, e2203855119 (2022).
932 23. Kienle, K. *et al.* Neutrophils self-limit swarming to contain bacterial growth in vivo.
933 *Science* **372**, eabe7729 (2021).
934 24. Song, Z., Bhattacharya, S., Clemens, R. A. & Dinauer, M. C. Molecular regulation of
935 neutrophil swarming in health and disease: Lessons from the phagocyte oxidase.
936 *iScience* **26**, 108034 (2023).
937 25. Uderhardt, S., Martins, A. J., Tsang, J. S., Lämmermann, T. & Germain, R. N. Resident
938 Macrophages Cloak Tissue Microlesions to Prevent Neutrophil-Driven Inflammatory
939 Damage. *Cell* **177**, 541-555.e17 (2019).
940 26. Lämmermann, T. In the eye of the neutrophil swarm—navigation signals that bring
941 neutrophils together in inflamed and infected tissues. *J. Leukoc. Biol.* **100**, 55–63
942 (2016).
943 27. Netea, M. G. *et al.* Defining trained immunity and its role in health and disease. *Nat.*
944 *Rev. Immunol.* **20**, 375–388 (2020).
945 28. Kleinnijenhuis, J. *et al.* Bacille Calmette-Guérin induces NOD2-dependent
946 nonspecific protection from reinfection via epigenetic reprogramming of
947 monocytes. *Proc. Natl. Acad. Sci.* **109**, 17537–17542 (2012).
948 29. Quintin, J. *et al.* Candida albicans Infection Affords Protection against Reinfection
949 via Functional Reprogramming of Monocytes. *Cell Host Microbe* **12**, 223–232 (2012).
950 30. Kalafati, L. *et al.* Innate Immune Training of Granulopoiesis Promotes Anti-tumor
951 Activity. *Cell* **183**, 771-785.e12 (2020).

31. Kato, Y. & Kumanogoh, A. The immune memory of innate immune systems. *Int. Immunol.* **37**, 195–202 (2025).

32. Mitroulis, I. *et al.* Modulation of Myelopoiesis Progenitors Is an Integral Component of Trained Immunity. *Cell* **172**, 147-161.e12 (2018).

33. Kaufmann, E. *et al.* BCG Educates Hematopoietic Stem Cells to Generate Protective Innate Immunity against Tuberculosis. *Cell* **172**, 176-190.e19 (2018).

34. Schlüter, T., Van Elsas, Y., Priem, B., Ziogas, A. & Netea, M. G. Trained immunity: induction of an inflammatory memory in disease. *Cell Res.* https://doi.org/10.1038/s41422-025-01171-y (2025) doi:10.1038/s41422-025-01171-y.

35. Fanucchi, S., Domínguez-Andrés, J., Joosten, L. A. B., Netea, M. G. & Mhlanga, M. M. The Intersection of Epigenetics and Metabolism in Trained Immunity. *Immunity* **54**, 32–43 (2021).

36. Darroch, H. *et al.* Infection-experienced HSPCs protect against infections by generating neutrophils with enhanced mitochondrial bactericidal activity. *Sci. Adv.* **9**, eadf9904 (2023).

37. Mariotti, B. *et al.* Innate immune reprogramming in circulating neutrophils of COPD patients. *J. Allergy Clin. Immunol.* **156**, 373–384 (2025).

38. Gomes, M. C., Brokatzky, D., Bielecka, M. K., Wardle, F. C. & Mostowy, S. *Shigella* induces epigenetic reprogramming of zebrafish neutrophils. *Sci. Adv.* **9**, eadf9706 (2023).

39. Patel, K. K., Tariveranmoshabad, M., Kadu, S., Shobaki, N. & June, C. From concept to cure: The evolution of CAR-T cell therapy. *Mol. Ther.* **33**, 2123–2140 (2025).

40. Abdin, S. M., Paasch, D. & Lachmann, N. CAR macrophages on a fast track to solid tumor therapy. *Nat. Immunol.* **25**, 11–12 (2024).

41. Chang, Y. *et al.* CAR-neutrophil mediated delivery of tumor-microenvironment responsive nanodrugs for glioblastoma chemo-immunotherapy. *Nat. Commun.* **14**, 2266 (2023).

42. Chang, Y. *et al.* Engineering chimeric antigen receptor neutrophils from human pluripotent stem cells for targeted cancer immunotherapy. *Cell Rep.* **40**, 111128 (2022).

43. Majumder, A. *et al.* iPSC-Derived CAR Neutrophils Possess Potent Activity Against Solid Tumors In Vivo. *Blood* **144**, 86–86 (2024).

44. Sathe, N. *et al.* Pseudomonas aeruginosa: Infections and novel approaches to treatment "Knowing the enemy" the threat of Pseudomonas aeruginosa and exploring novel approaches to treatment. *Infect. Med.* **2**, 178–194 (2023).

45. Ruffin, M. & Brochiero, E. Repair Process Impairment by Pseudomonas aeruginosa in Epithelial Tissues: Major Features and Potential Therapeutic Avenues. *Front. Cell. Infect. Microbiol.* **9**, 182 (2019).

46. Clatworthy, A. E. *et al.* *Pseudomonas aeruginosa* Infection of Zebrafish Involves both Host and Pathogen Determinants. *Infect. Immun.* **77**, 1293–1303 (2009).

47. Gault, W. J., Enyedi, B. & Niethammer, P. Osmotic surveillance mediates rapid wound closure through nucleotide release. *J. Cell Biol.* **207**, 767–782 (2014).

48. Enyedi, B., Kala, S., Nikolich-Zugich, T. & Niethammer, P. Tissue damage detection by osmotic surveillance. *Nat. Cell Biol.* **15**, 1123–1130 (2013).

49. Huang, C. & Niethammer, P. Tissue Damage Signaling Is a Prerequisite for Protective Neutrophil Recruitment to Microbial Infection in Zebrafish. *Immunity* **48**, 1006-1013.e6 (2018).

50. Williantarra, I., Georgantzoglou, A. & Sarris, M. Visualising Neutrophil Actin Dynamics in Zebrafish in Response to Laser Wounding Using Two-Photon Microscopy. *BIO-Protoc.* **14**, (2024).

51. LaBauve, A. E. & Wargo, M. J. Growth and Laboratory Maintenance of *Pseudomonas aeruginosa*. *Curr. Protoc. Microbiol.* **25**, (2012).

52. Potvin-Trottier, L., Lord, N. D., Vinnicombe, G. & Paulsson, J. Synchronous long-term oscillations in a synthetic gene circuit. *Nature* **538**, 514–517 (2016).

53. Devanga Ragupathi, N. K., Muthuirulandi Sethuvel, D. P., Inbanathan, F. Y. & Veeraraghavan, B. Accurate differentiation of Escherichia coli and Shigella serogroups: challenges and strategies. *New Microbes New Infect.* **21**, 58–62 (2018).

54. Park, S. A., Choe, Y. H., Park, E. & Hyun, Y.-M. Real-time dynamics of neutrophil clustering in response to phototoxicity-induced cell death and tissue damage in mouse ear dermis. *Cell Adhes. Migr.* 1–20 (2018) doi:10.1080/19336918.2018.1471322.

55. Malet-Engra, G. *et al.* Collective Cell Motility Promotes Chemotactic Prowess and Resistance to Chemorepulsion. *Curr. Biol.* **25**, 242–250 (2015).

56. Cai, D. *et al.* Modeling and analysis of collective cell migration in an in vivo three-dimensional environment. *Proc. Natl. Acad. Sci.* **113**, (2016).

57. Murphy, R. C. & Gijón, M. A. Biosynthesis and metabolism of leukotrienes. *Biochem. J.* **405**, 379–395 (2007).

58. Horn, A. *et al.* Isotonic medium treatment limits burn wound microbial colonisation and improves tissue repair. *Wound Repair Regen.* **33**, e13242 (2025).

59. Kazmierczak, B. I., Schniederberend, M. & Jain, R. Cross-regulation of Pseudomonas motility systems: the intimate relationship between flagella, pili and virulence. *Curr. Opin. Microbiol.* **28**, 78–82 (2015).

60. Huang, L. *et al.* Engineered probiotic Escherichia coli elicits immediate and long-term protection against influenza A virus in mice. *Nat. Commun.* **15**, 6802 (2024).

61. Moorlag, S. J. C. F. M. *et al.* Multi-omics analysis of innate and adaptive responses to BCG vaccination reveals epigenetic cell states that predict trained immunity. *Immunity* **57**, 171-187.e14 (2024).

62. Wang, X. *et al.* Endotoxin-induced autocrine ATP signaling inhibits neutrophil chemotaxis through enhancing myosin light chain phosphorylation. *Proc. Natl. Acad. Sci.* **114**, 4483–4488 (2017).

63. Wang, W. *et al.* Breakthrough of solid tumor treatment: CAR-NK immunotherapy. *Cell Death Discov.* **10**, 40 (2024).

64. Sterner, R. C. & Sterner, R. M. CAR-T cell therapy: current limitations and potential strategies. *Blood Cancer J.* **11**, 69 (2021).

65. Bradford, Y. M. *et al.* Zebrafish information network, the knowledgebase for *Danio rerio* research. *Genetics* **220**, iyac016 (2022).

66. Renshaw, S. A. *et al.* A transgenic zebrafish model of neutrophilic inflammation. *Blood* **108**, 3976–3978 (2006).

67. Bakshi, S. *et al.* Tracking bacterial lineages in complex and dynamic environments with applications for growth control and persistence. *Nat. Microbiol.* **6**, 783–791 (2021).

68. Sarris, M. *et al*. Inflammatory Chemokines Direct and Restrict Leukocyte Migration within Live Tissues as Glycan-Bound Gradients. *Curr. Biol*. **22**, 2375–2382 (2012).

69. Livak, K. J. & Schmittgen, T. D. Analysis of Relative Gene Expression Data Using Real-Time Quantitative PCR and the 2−ΔΔCT Method. *Methods* **25**, 402–408 (2001).

1051 # Figure Legends

1052

1053 **Figure 1. Osmotic surveillance determines susceptibility to wound infection.**

1054

1055 A. Schematic detailing the mechanical wound (MW) wound-infection model by tail fin
1056 (TF) transection method in the presence of *P. aeruginosa* PAO1.
1057 B. Parameters assessed in the disease scoring matrix to accord a disease progression stage
1058 to each zebrafish larva.
1059 C. Disease progression in the specified group of larvae at the indicated time points.
1060 Representative of three independent experiments, with n ≥ 24 larvae per group.
1061 D. Bacterial burden of *P. aeruginosa* in the specified groups of zebrafish larvae at 24 hpi
1062 (hours post infection). CFU, colony forming units. (Representative of three independent
1063 experiments with n ≥9 larvae per group used for CFU analysis in each experiment).
1064 (mean ± SD). *One-way ANOVA with Tukey's multiple comparisons test,* ***$P < 0.001$
1065 E. Survival curves from zebrafish larvae when exposed to indicated buffers and *P.*
1066 *aeruginosa* infection upon MW. (Representative of three independent experiments with
1067 n ≥ 24 larvae per group for the wounded-infected; n ≥ 9 larvae per group for the non-
1068 wounded infected, in each experiment). *Log-rank (Mantel-Cox) test; ***$P < 0.001$*
1069 F. Bacterial burden of *P. aeruginosa* in the specified groups of zebrafish larvae at early
1070 time points (10 mins and 30 mins) of infection. (Representative of three independent
1071 experiments with n ≥ 12 larvae per group per time point in each experiment. (mean ±
1072 SD). CFU, colony forming units. *One-way ANOVA with, Šídák's multiple comparisons*
1073 *test,* **$P < 0.01$
1074 G. Schematic detailing the laser wound (LW) infection model. CHT: caudal hematopoietic
1075 tissue; VF: ventral fin.
1076 H. Survival curves from zebrafish larvae when exposed to indicated buffers and *P.*
1077 *aeruginosa* infection upon LW. (Representative of three independent experiments with
1078 n ≥ 24 larvae per group for the wounded-infected; n≥12 larvae per group for the non-
1079 wounded infected, in each experiment). *Log-rank (Mantel-Cox) test,* *$P < 0.05$
1080 I. Bacterial burden of *P. aeruginosa* in the specified groups of zebrafish larvae at 24 hpi
1081 (hours post infection). Representative of three independent experiments, with n ≥12
1082 larvae per group in each experiment. (mean ± SD). CFU, colony forming units.
1083 *Unpaired t test,* *$P < 0.05$

1084 J. Disease progression in the specified group of larvae at the indicated time points.
1085 Representative of three independent experiments with n ≥ 24 larvae per group.
1086
1087 **Figure 2: Immune training enhances resistance to wound infections and reprograms**
1088 **genes associated to swarming.**
1089
1090 A. Schematic of the training experiment. Zebrafish larvae pre-challenged by PBS or a dose
1091 of *E. coli* in the otic vesicle (OV) at 2 days post fertilization (dpf) stage and
1092 subsequently subjected to mechanical wounding in the tail fin (TF) and *P. aeruginosa*
1093 PAO1 infection at 4 dpf.
1094 B. Survival curves from control (PBS) and trained (EC) zebrafish larvae upon *P.*
1095 *aeruginosa* infection following MW. (Representative of three independent experiments
1096 with n ≥ 36 larvae per group in each experiment). *Log-rank (Mantel-Cox) test; ****P*
1097 *< 0.0001.*
1098 C. Bacterial burden of *P. aeruginosa* in the control and trained zebrafish larvae at 24 hpi
1099 (hours post infection). (Representative of three independent experiments, with n ≥ 9
1100 larvae per group used for CFU analysis in each experiment. (mean ± SD). CFU, colony
1101 forming units. *One-way ANOVA with Tukey's multiple comparisons test, *P < 0.05*
1102 D. Disease progression in the control and trained zebrafish larvae at the indicated time
1103 points. Representative of three independent experiments with n ≥ 36 larvae per group
1104 in each experiment.
1105 E. Schematic detailing the assessment of *E. coli* burden and cytokine profile in whole
1106 zebrafish larvae after primary challenge (PBS/ *E. coli*) for trained immunity induction.
1107 F. Bacterial counts at the indicated time points after injection of *E. coli* in the otic vesicle
1108 (OV) of the zebrafish larvae. Representative of three independent experiments, with n
1109 ≥ 12 larvae for each time point.
1110 G-J. Change in the expression profile of the indicated cytokines in naive and trained
1111 zebrafish larvae at the specific time points after primary challenge. Representative of
1112 three independent experiments, with n ≥ 8 larvae at each time point.
1113 K. Schematic describing the isolation of neutrophils by Fluorescence Activated Cell
1114 Sorting (FACS) from the hematopoietic site (CHT: Caudal hematopoietic tissue) of
1115 zebrafish larvae, followed by transcript analysis using RT-PCR.
1116 L-R. Change in the expression profile of the indicated genes in naive and trained zebrafish
1117 larvae at 4dpf (2 days after primary challenge). Quantitative PCR data are presented as

mean ± S.E.M., with expression levels normalised to PBS-treated control groups (n=5 independent experiments, with each replicate representing a pool of 150-200 larvae at 4 dpf). Statistical significance was assessed using the Mann-Whitney test/ t-test (*$p < 0.05$, **$p < 0.01$).

Figure 3 Immune training induces alterations in neutrophil swarming that are beneficial for bacterial defence

A. Schematic of experiment with control, PBS pre-challenged or trained, E. Coli pre-challenged (EC) zebrafish larvae subjected to laser wounding (LW), followed by infection with P. aeruginosa (PAO1) and simultaneous confocal imaging.
B. Time lapse images of representative movies of control and trained larvae at 1 min prior LW (-1 min), at the time of LW (0 min), at 30 min and 90 min post LW. White dashed lines correspond to the CHT: caudal hematopoietic tissue and VF: ventral fin. Red dashed lines correspond to the site of the LW. On the far-right, neutrophil trajectories of same movie are depicted wherein each colour corresponds to a different neutrophil trajectory. Scale bar 50 µm.
C. Radial speed quantification of tracked cells in control (PBS) (black) and trained EC animals (pink) overtime after laser wound and infection. To reduce noise moving average with overlapping window of 3 point was used. Multiple unpaired t test ** $p < 0.01$.
D. Summary of individual larva-based analyses of control (PBS) (black) and trained (EC) animals (pink). The y-axis on the graph depicts bacterial burden in larva at 24 hours post infection (hpi) (after LW and infection), and the x-axis indicates the average radial speed 60-120 minutes post LW. Thresholds are set at the minimum PAO1 CFU value in which disease symptoms were observed (stage 1 or above, diamond shape), and the mean radial speed of all the animals in the same interval. Black rectangles and text indicate the movies used for representative images in B. Different shapes show the individual disease stages of each larva.
E. Contingency analysis of groups in D. n=16 (PBS) and n=17 (EC). Fisher's exact test * $p < 0.05$.

F-G. Survival curves from control (PBS) and trained (EC) zebrafish larvae upon PAO1 infection following mechanical wound. Larvae were pre-treated with DMSO or 20µM Zileuton (Zil), 1h prior to wounding and kept in this medium until the end of the

experiment Representative of three independent experiments with n ≥28 larvae per group for each experiment in E, and n ≥ 20 larvae in F. Log-rank (Mantel-Cox) test; * $p < 0.05$, ns $p > 0.05$.

H-I. Bacterial burden of P. aeruginosa in larvae from groups in E and F respectively. Representative of three independent experiments with n ≥ 9 larvae per group used for CFU analysis in each experiment. (mean ± SD). CFU, colony forming units. Unpaired t test with Welch's correction. * $p < 0.05$, ns $p > 0.05$.

Figure 4: Genetic enhancement of neutrophil LTB4 synthesis is sufficient to alter neutrophil swarm kinetics and infection outcome.

A. Survival curves from control (CTR) zebrafish larvae and larvae overexpressing 5-LO in neutrophils (5-LO-Neu) upon *P. aeruginosa* infection following MW. Representative of three independent experiments with n ≥ 50 larvae per group in each experiment. *Log-rank (Mantel-Cox) test; * $p < 0.05$.*
B. Bacterial burden of fish in survival experiments (A). Representative of three independent experiments with n ≥ 9 larvae per group used for CFU analysis in each experiment. *Unpaired t test with Welch's correction; * $p < 0.05$, ** $p < 0.01$.*
C. Disease progression in the specified group of larvae at the indicated time points. Representative of three independent experiments with n ≥ 50 larvae per group in each experiment.
D. Time lapse images of representative movies of CTR and 5-LO-Neu at 1 min prior to LW (-1 min), at the time of LW (0 min), at 30 min and 90 min after LW. White dashed lines indicated the CHT: caudal hematopoietic tissue and VF: ventral fin. Red dashed line corresponds to the site of the laser wound (LW). On the right column neutrophil trajectories of same movie are represented wherein each colour indicates a different neutrophil trajectory. Scale bar 50 µm.
E. Radial speed quantification of tracked cells in control (CTR) (*black*) and 5-LO-Neu animals *(pink)* overtime after laser wound and infection. To reduce noise moving average with overlapping window of 3 point was used *Multiple unpaired t-test. *** $p < 0.001$.*
F. Summary of individual larva-based analyses of control (CTR) *(black)* and 5-LO-Neu animals *(pink)*. The y-axis on the graph depicts bacterial burden in larva at 24 hours post infection (hpi) (after LW and infection), and the x-axis indicates the average radial

speed 25-60 minutes post LW. Thresholds are set at the minimum PAO1 CFU value in which disease symptoms were observed (stage 1 or above, diamond shape), and the mean radial speed of all the animals in the same interval. Black rectangles and text indicate the movies used for representative images in D. Different shapes show the individual disease stages of each larva.

G. Contingency analysis of groups in F. n=15 (CTR) and n=18 (5-LO-Neu). *Fisher's exact test* * $p < 0.05$.

Figure 5: Mathematical modelling predicts how variation in neutrophil chemoattractant secretion influences bacterial clearance.

A. Schematic of the simulated domain around the wound. Cells are initially placed randomly with uniform average density, and have a net migration speed towards the wound given by Eqs.(1,2). The simulated domain is bounded at its centre by the wound (red circle), where cells accumulate. At the outer boundary (green dashed line), there is an influx of cells, at random places around the edge, to maintain the density at the edge constant on average. The bottom panel explains how we calculate the average chemotactic cell speed by the difference between the traction forces at the opposing ends of the cell, with respect to the wound direction (Eq.2).

B. Snapshots of the simulated cells during an example of a recruitment process, with cells arriving in the wound (red) secreting chemoattractant.

C. heatmap giving the speed towards the wound at different locations, at the same times of (B).

D. Time series of the accumulated number of immune cells arriving in the wound (black line) and number of bacteria (blue line) from the example in (B,C) (see Movie S4).

E. Results of 40 simulations of different random initial conditions, for several values of the chemoattractant secretion strength parameter α (Eq.3). We plot the log of the number of bacteria (Eq.9) and number of recruited neutrophils that arrived at the wound by the final time of the simulation (100 min). The point highlighted by a square corresponds to the example of the recruitment process shown in (B-D). In the inset we show the mean values of these scatter clouds.

F. Mean number of recruited immune cells as function of time, for the different values of α in (E).

G. As in (F), for the mean number of bacteria.

H. Average speed towards the wound as function of time, for the cells outside the wound, normalized by the value of the first peak of the WT cells (black line). Pink and green lines give the data for the 5LO and E-coli-treated fish respectively.

I. As in (H) from the simulations, for the following parameter values: WT-like: α=10, 5LO-like: α=35, E. coli-like: $\alpha_0 = 11$, $\alpha_1 = 89$ with B_s =350.

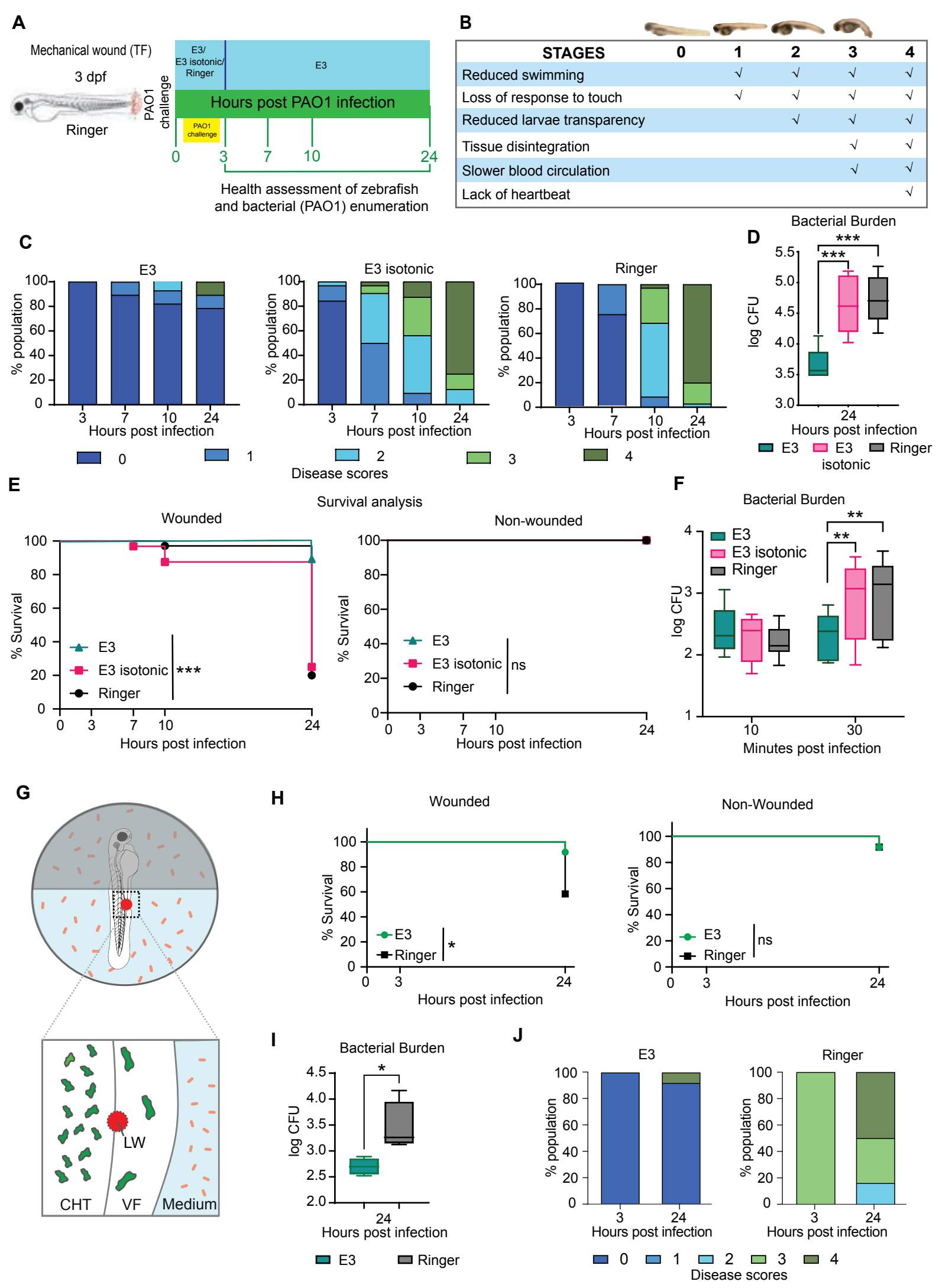
A
Mechanical wound (TF)
3 dpf
Ringer
PAO1 challenge
E3/ E3 isotonic/ Ringer
E3
Hours post PAO1 infection
PAO1 challenge
0
3
7
10
24
Health assessment of zebrafish and bacterial (PAO1) enumeration
B
STAGES
0
1
2
3
4
Reduced swimming
Loss of response to touch
Reduced larvae transparency
Tissue disintegration
Slower blood circulation
Lack of heartbeat
C
E3
E3 isotonic
Ringer
% population
Hours post infection
Disease scores
D
Bacterial Burden
log CFU
Hours post infection
E3
E3 isotonic
Ringer
E
Survival analysis
Wounded
Non-wounded
% Survival
Hours post infection
***
ns
F
Bacterial Burden
log CFU
Minutes post infection
**
G
LW
CHT
VF
Medium
H
Wounded
Non-Wounded
% Survival
Hours post infection
*
ns
I
Bacterial Burden
log CFU
Hours post infection
E3
Ringer
J
E3
Ringer
% population
Hours post infection
Disease scores

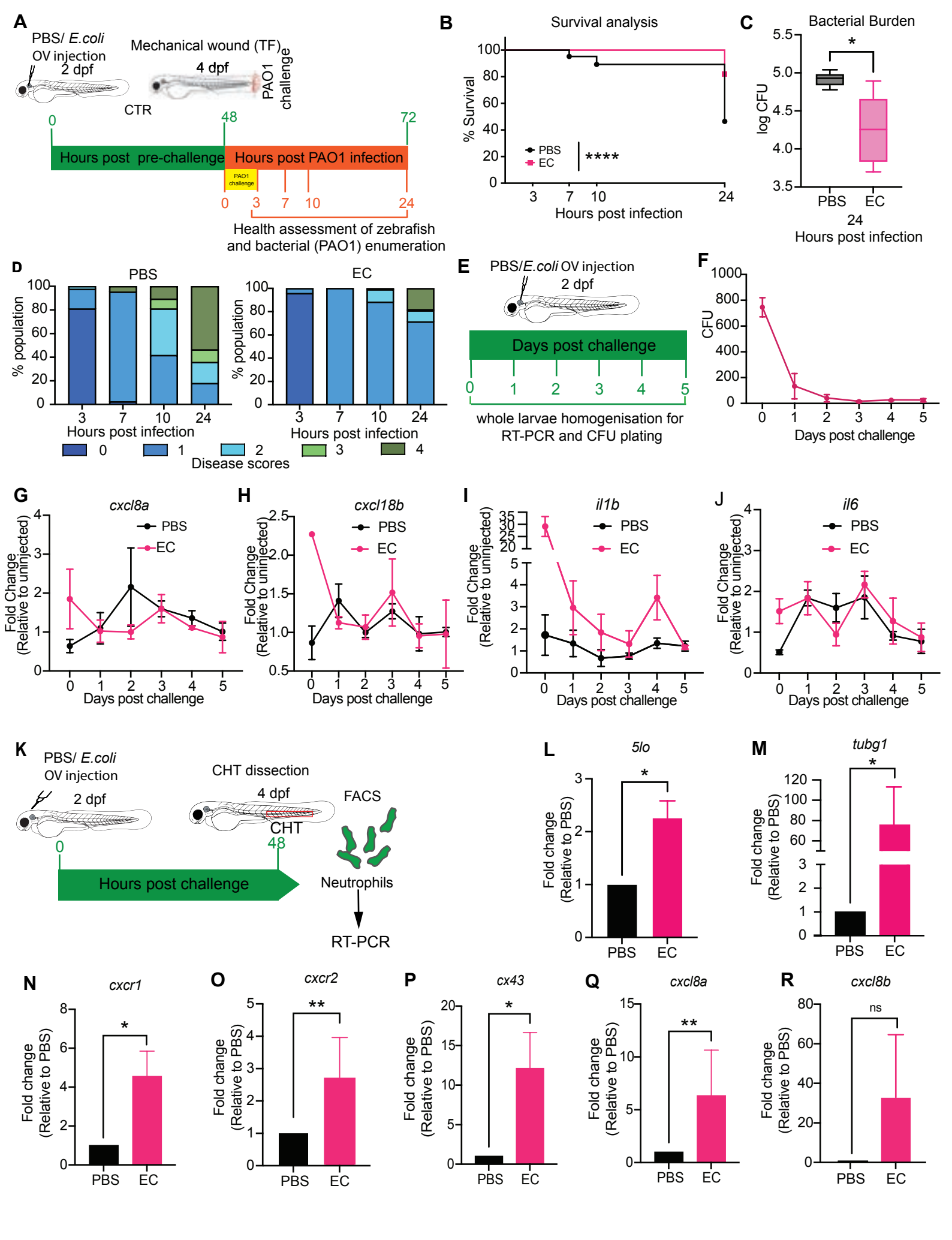
A
PBS/ E.coli
OV injection
2 dpf
Mechanical wound (TF)
4 dpf
PAO1
challenge
CTR
0
48
72
Hours post pre-challenge
Hours post PAO1 infection
PAO1 challenge
0 3 7 10 24
Health assessment of zebrafish and bacterial (PAO1) enumeration
B
Survival analysis
% Survival
PBS
EC
****
Hours post infection
C
Bacterial Burden
log CFU
PBS
EC
24
Hours post infection
D
PBS
EC
% population
Hours post infection
Disease scores
E
PBS/E.coli OV injection
2 dpf
Days post challenge
whole larvae homogenisation for RT-PCR and CFU plating
F
CFU
Days post challenge
G
cxcl8a
Fold Change (Relative to uninjected)
Days post challenge
H
cxcl18b
I
il1b
J
il6
K
PBS/ E.coli
OV injection
2 dpf
CHT dissection
4 dpf
CHT
FACS
Hours post challenge
Neutrophils
RT-PCR
L
5lo
Fold change (Relative to PBS)
M
tubg1
N
cxcr1
O
cxcr2
P
cx43
Q
cxcl8a
R
cxcl8b
ns

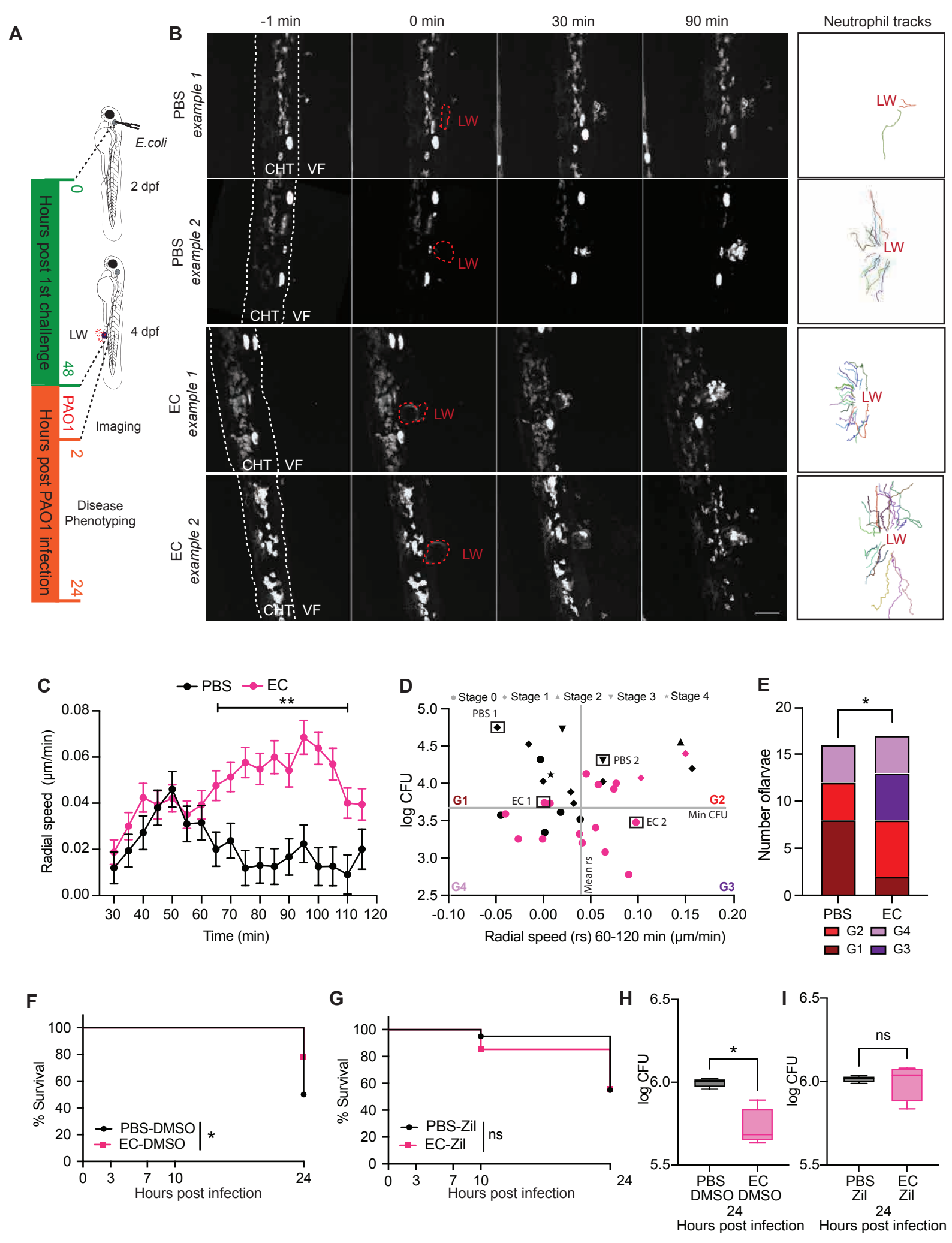
A
E.coli
2 dpf
4 dpf
LW
Imaging
Disease Phenotyping
Hours post 1st challenge
Hours post PAO1 infection
0
48
PAO1
2
24
B
-1 min
0 min
30 min
90 min
Neutrophil tracks
PBS example 1
PBS example 2
EC example 1
EC example 2
CHT
VF
LW
C
PBS
EC
**
Radial speed (µm/min)
Time (min)
D
Stage 0
Stage 1
Stage 2
Stage 3
Stage 4
PBS 1
PBS 2
EC 1
EC 2
G1
G2
G3
G4
Min CFU
Mean rs
log CFU
Radial speed (rs) 60-120 min (µm/min)
E
*
Number oflarvae
PBS
EC
G2
G4
G1
G3
F
% Survival
PBS-DMSO
EC-DMSO
*
Hours post infection
G
% Survival
PBS-Zil
EC-Zil
ns
Hours post infection
H
log CFU
*
PBS DMSO
EC DMSO
24
Hours post infection
I
log CFU
ns
PBS Zil
EC Zil
24
Hours post infection

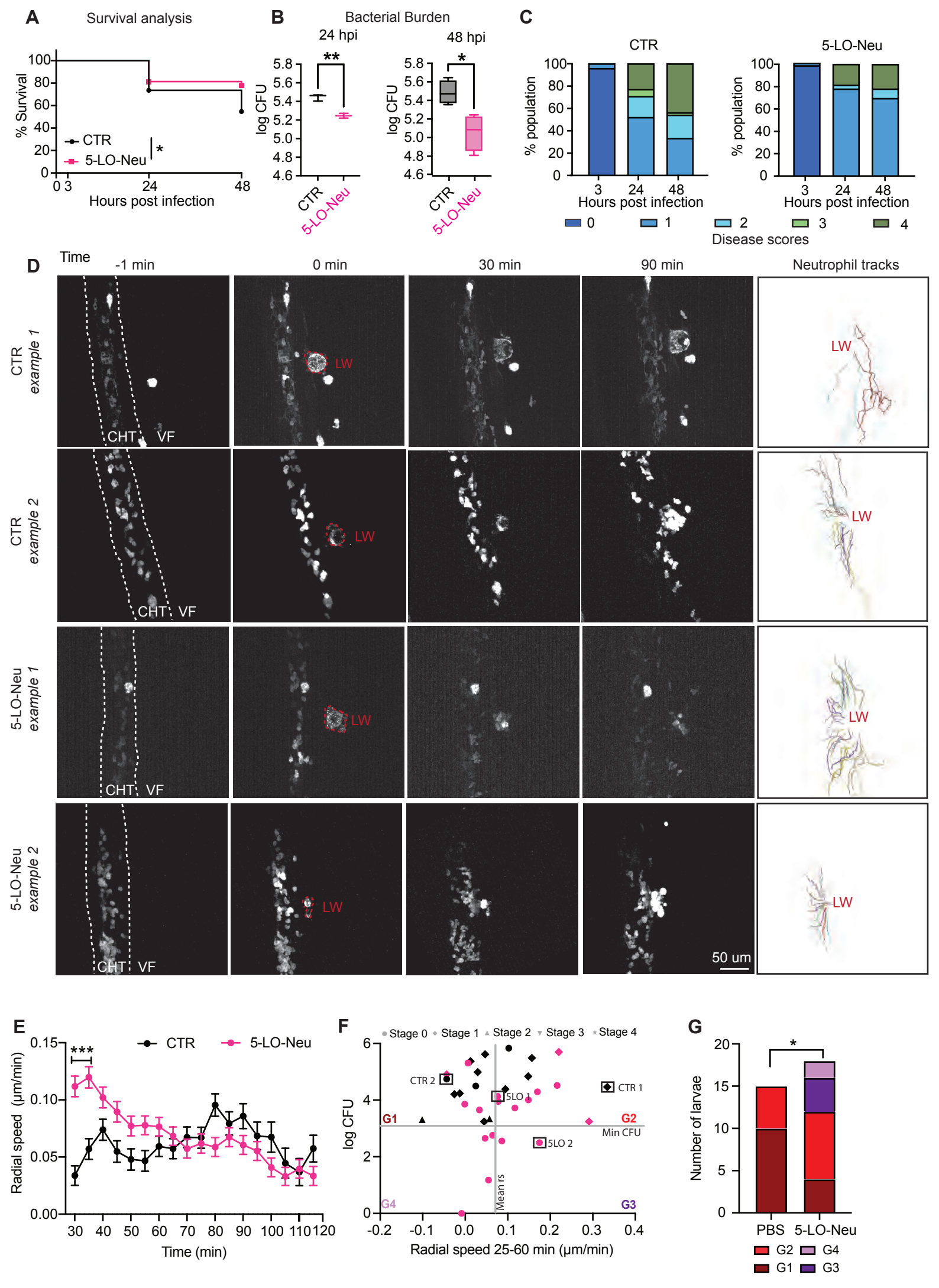
A
Survival analysis
% Survival
CTR
5-LO-Neu
*
Hours post infection
B
Bacterial Burden
24 hpi
48 hpi
log CFU
**
*
CTR
5-LO-Neu
C
CTR
5-LO-Neu
% population
Hours post infection
Disease scores
D
Time
-1 min
0 min
30 min
90 min
Neutrophil tracks
CTR example 1
CTR example 2
5-LO-Neu example 1
5-LO-Neu example 2
CHT
VF
LW
50 um
E
Radial speed (µm/min)
Time (min)
***
F
Stage 0
Stage 1
Stage 2
Stage 3
Stage 4
log CFU
CTR 1
CTR 2
5LO 1
5LO 2
G1
G2
G3
G4
Min CFU
Mean rs
Radial speed 25-60 min (µm/min)
G
Number of larvae
PBS
5-LO-Neu
G2
G4
G1
G3

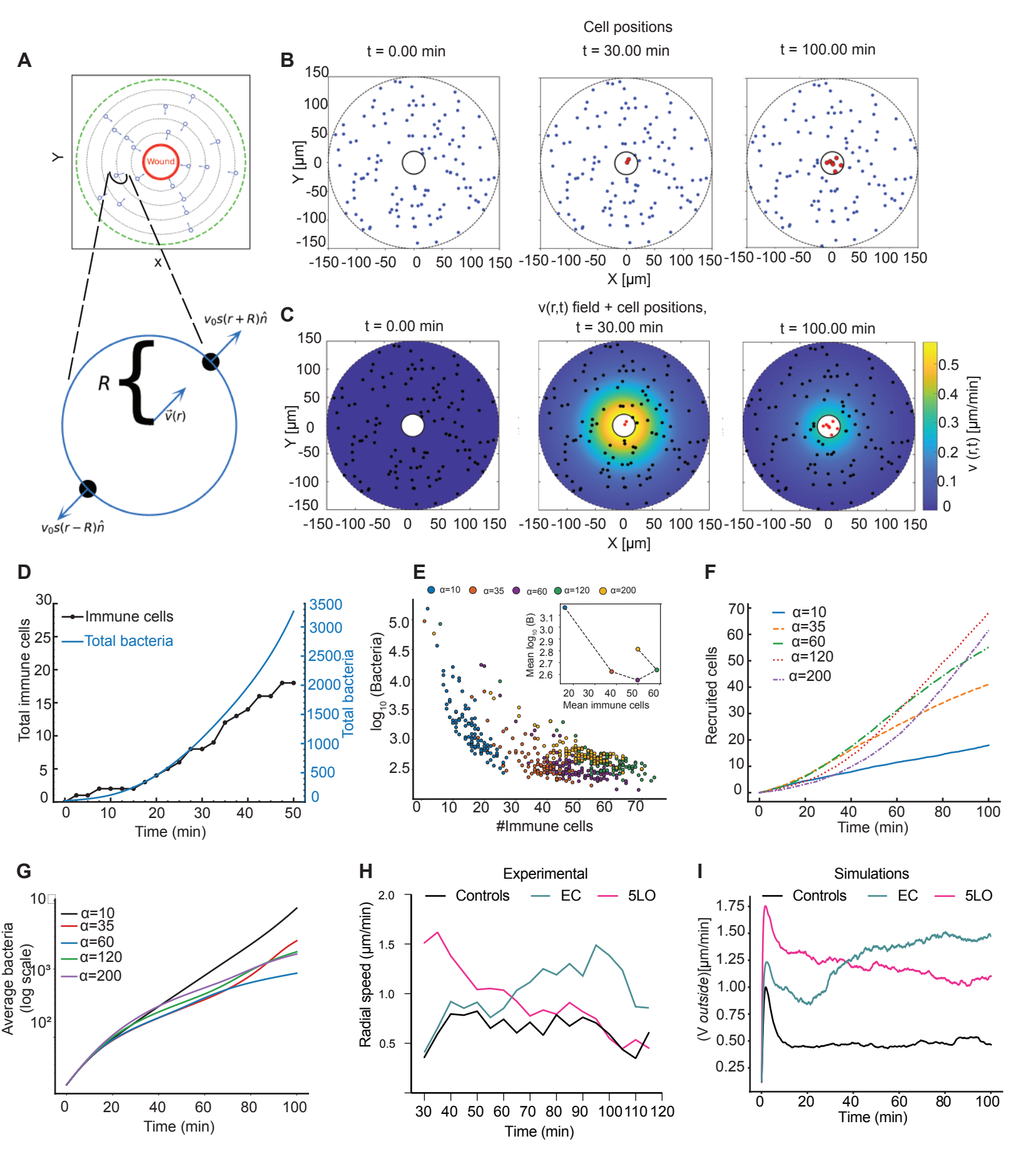
A
Wound
Y
x
$v_0 s(r+R)\hat{n}$
R
$\vec{v}(r)$
$v_0 s(r-R)\hat{n}$
B
Cell positions
t = 0.00 min
t = 30.00 min
t = 100.00 min
Y [μm]
X [μm]
C
v(r,t) field + cell positions,
t = 0.00 min
t = 30.00 min
t = 100.00 min
Y [μm]
X [μm]
v (r,t) [μm/min]
D
Immune cells
Total bacteria
Total immune cells
Total bacteria
Time (min)
E
α=10
α=35
α=60
α=120
α=200
$\log_{10}$ (Bacteria)
#Immune cells
Mean $\log_{10}$ (B)
Mean immune cells
F
α=10
α=35
α=60
α=120
α=200
Recruited cells
Time (min)
G
α=10
α=35
α=60
α=120
α=200
Average bacteria (log scale)
Time (min)
H
Experimental
Controls
EC
5LO
Radial speed (μm/min)
Time (min)
I
Simulations
Controls
EC
5LO
(V outside)[μm/min]
Time (min)